Journal of Translational Medicine

RESEARCH

Open Access

Mfn2 regulates calcium homeostasis and suppresses PASMCs proliferation via interaction with IP3R3 to mitigate pulmonary arterial hypertension

Rui Wang[1†], Jie Wang[2†], Jing Yu[3], Zhiqiang Li[4], Minfang Zhang[5], Yuhu Chen[6], Fen Liu[7], Dongmei Jiang[1], Jingfei Guo[1], Xiaomei Li[8*] and Yun Wu[1*]

Abstract

Background Pulmonary arterial hypertension (PAH) is a chronic disorder characterized by the excessive proliferation of pulmonary arterial smooth muscle cells (PASMCs). Recent studies indicate that Mitochondrial fusion protein 2 (Mfn2) maintains intracellular calcium (Ca^{2+}) homeostasis via the mitochondria-associated endoplasmic reticulum membranes (MAMs) pathway, thereby inhibiting PASMCs proliferation and reducing pulmonary artery pressure. However, the precise mechanisms remain unclear.

Methods This study explored the roles of Mfn2 and IP3R3 in PAH progression by assessing their expression in lung tissues of a monocrotaline (MCT)-induced PAH rat model. Immunoprecipitation assays were performed to confirm the interaction between Mfn2 and IP3R3. PASMCs were treated with either silenced or overexpressed Mfn2 and exposed to TNF-α to observe effects on ER stress, IP3R3 expression, mitochondrial Ca^{2+} transport, and mitochondrial integrity. We also evaluated the effects of 4-phenylbutyric acid (4-PBA) and cistanche phenylethanol glycosides (CPGs) on the Mfn2-IP3R3 interaction in a TNF-α-induced PAH cell model, focusing on Ca^{2+} transport and mitochondrial structure.

Results Mfn2 expression was significantly down-regulated in the MCT-induced PAH rat model. Inhibition of ER stress upregulated Mfn2 expression, downregulated IP3R3 expression, increased mitochondrial Ca^{2+} concentration, and reduced autophagy, improving pulmonary hemodynamics and vascular remodeling. Overexpression of Mfn2 reduced ER stress, decreased IP3R3 expression, decreased mitochondrial Ca^{2+} transport, and restored mitochondrial integrity. Immunoprecipitation assays confirmed the interaction between Mfn2 and IP3R3. Inhibition of IP3R3 elevated Mfn2 levels, yielding similar beneficial effects as Mfn2 overexpression. 4-PBA and CPGs modulated the Mfn2-IP3R3 signaling axis, effectively inhibiting PAH progression.

†Rui Wang and Jie Wang contributed equally to this work and shared the first authorship.

*Correspondence:
Xiaomei Li
lixm505@163.com
Yun Wu
wuyun8009@163.com

Full list of author information is available at the end of the article

Conclusions Mfn2 mediates mitochondrial Ca^{2+} transport via IP3R3, suppressing PASMCs proliferation and pulmonary vascular remodeling, underscoring Mfn2's potential in regulating metabolic processes and vascular remodeling in PAH. These findings provide new insights for developing PAH-targeted therapeutics and establish a theoretical basis for traditional Chinese medicine in PAH prevention and treatment.

Graphical Abstract

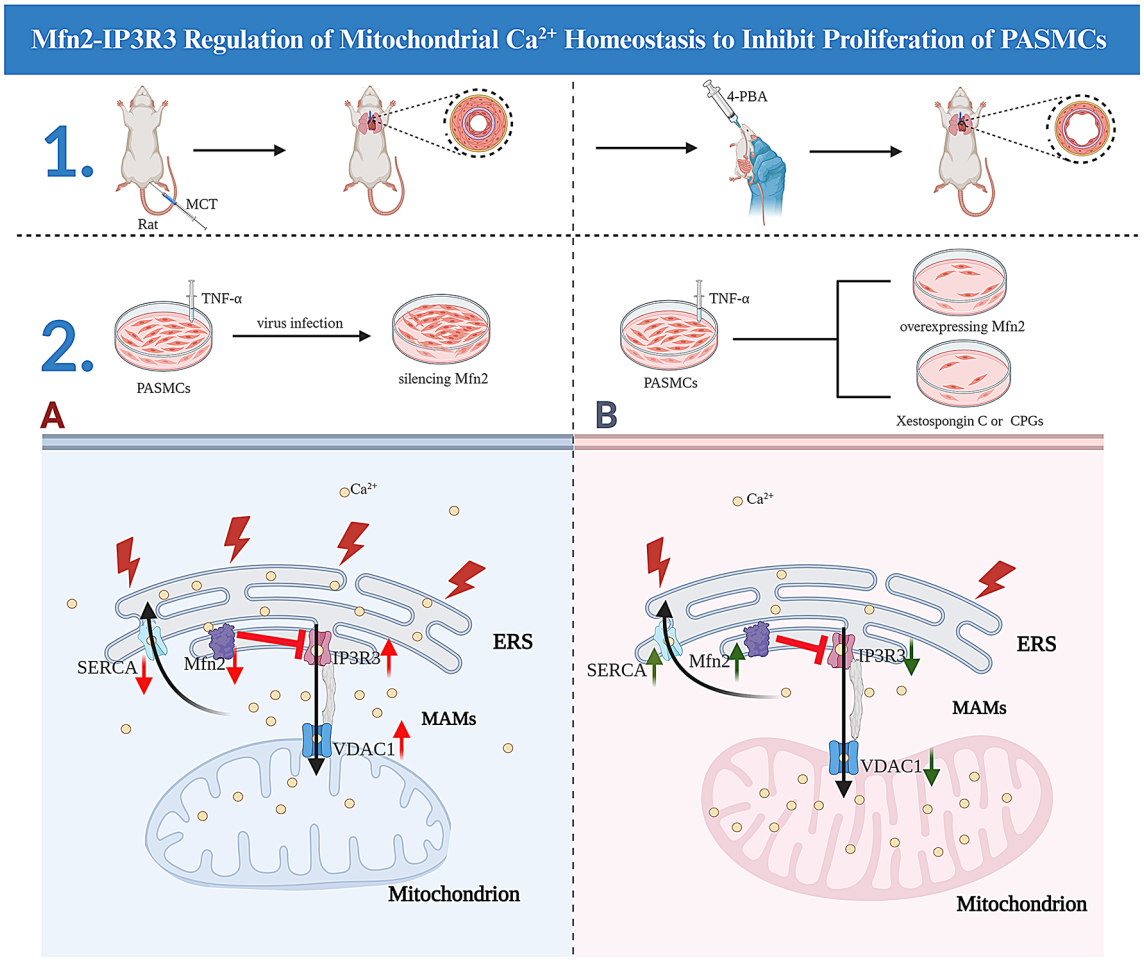

Keywords Pulmonary artery hypertension, Endoplasmic reticulum stress, Mitochondrial autophagy, Mfn2 interact with IP3R3, Ca^{2+} homeostasis

Introduction

Pulmonary arterial hypertension (PAH) is a life-threatening cardiopulmonary disease characterized by abnormal contraction of the pulmonary arteries and vascular remodeling, which eventually leads to right heart failure and death. The incidence of PAH is approximately 7.6 cases per million, with a prevalence between 11 and 26 cases per million [1, 2]. Studies have shown that irreversible pulmonary vascular remodeling results from changes in the cells of the arterial vessel walls, particularly the excessive proliferation and migration of pulmonary artery smooth muscle cells (PASMCs) [3]. Currently, there is no effective way to reverse disease progression. Existing treatment strategies provide symptomatic relief but do not significantly reduce morbidity and mortality, resulting in poor patient outcomes [4]. Therefore, novel molecular or signaling pathways targeting pulmonary artery remodeling and PASMCs proliferation are urgently needed to identify new therapeutic targets.

Mitochondrial fusion protein 2 (MFN2), a dynamin-related protein with Guanosine Triphosphatase (GTPase) activity, is predominantly located in the outer mitochondrial membrane and the mitochondria-associated endoplasmic reticulum membranes (MAMs) [5]. Several

studies have shown that MFN2 is crucial for maintaining calcium (Ca^{2+}) transport, lipid metabolism, and glucose metabolism by tethering the endoplasmic reticulum (ER) and mitochondria together [6]. In addition, MFN2 can balance mitochondrial fusion and fission [7, 8]. Previously, our group demonstrated that Mfn2 plays a critical role in inhibiting PASMCs proliferation, with reduced Mfn2 expression observed in the monocrotaline (MCT)-induced PAH rat model, accompanied by increased mitochondrial autophagy and ER stress [9]. However, the precise mechanism through which Mfn2 influences PAH progression remains unclear and warrants further investigation.

The concentration of Ca^{2+} in PASMCs plays a crucial role in regulating vasoconstriction and vascular remodeling in pulmonary arteries, which is closely linked to the progression of PAH. Elevated cytoplasmic free Ca^{2+} concentrations can induce pulmonary artery vasoconstriction, promote PASMCs proliferation, and lead to vessel wall thickening [10–12]. The primary channel proteins involved in Ca^{2+} transport at the mitochondria-associated membranes (MAMs) are inositol 1,4,5-trisphosphate receptors (IP3Rs) and ryanodine receptors (RyRs). Several studies have reported that IP3R serves as an intracellular Ca^{2+} release channel and that increased intracellular Ca^{2+} contributes to pulmonary vasoconstriction, exacerbating PAH progression [13, 14]. Recent studies have indicated that during ER stress, activation of IP3Rs results in substantial Ca^{2+} release from the ER into the cytoplasm, leading to mitochondrial fragmentation and cellular proliferation [15, 16]. Despite these individual roles, PAH's potential crosstalk and coordinated functions of Mfn2 and type 3 inositol 1,4,5-triphosphate receptor (IP3R3) remain largely uninvestigated.

To further validate our previous hypotheses, we aim to elucidate the molecular mechanism by which Mfn2 binds to IP3R3 at MAMs to facilitate Ca^{2+} transport from the ER to the mitochondria. This study will be achieved by manipulating Mfn2 expression both in vivo, in the PAH rats model, and in vitro, in PASMCs cell models. Additionally, we will investigate the effects of CPG on PASMCs proliferation, a traditional herbal medicine from Xinjiang. Therefore, the study aims to enhance understanding of PAH pathogenesis and explore the anti-PAH mechanisms of CPG as a novel targeted therapy.

Materials and methods

Construction and grouping of experiment rats

Sixty male Wistar rats, weighing 180–200 g and aged 8–10 weeks, were obtained from the Department of Experimental Animal Science Research at the Medical Research Center of The First Affiliated Hospital of Xinjiang Medical University (*Experimental Animal Use License No. SYXK (Xin) 2010-0003*). All animal experiments were approved by the hospital's Institutional Animal Care and Use Committee prior to the study (*approval number: IACUC20190416-01*). The rats were housed under standard conditions (12-hour light/dark cycle, temperature range of 25–27℃, and humidity range of 50–70%) with ad libitum access to food and water.

A single intraperitoneal injection of 60 mg/kg monocrotaline (MCT) was administered to induce the PAH rat model. The mean pulmonary arterial pressure (mPAP) was measured using the BL-420 F bioinformatics acquisition system, with mPAP ≥ 25mmHg considered indicative of successful model establishment. The rats were subsequently divided into the following four groups: (1)Normal control group (NC group): normal rats received oral administration of 500 mg/(kg·d) physiological saline for 4 weeks. (2)PAH group: PAH rats received oral administration of 500 mg/(kg·d) physiological saline for 4 weeks. (3) Drug treatment group (REV group): PAH rats received oral administration of 500 mg/(kg·d) physiological saline for 2 weeks, followed by a suspension of 4-phenylbutyric acid (4-PBA) at a dose of 500 mg/(kg·d) for an additional 2 weeks. (4)Drug prevention group (PRE group): PAH rats received a suspension of 4-PBA at a dose of 500 mg/(kg·d) for 4 weeks.

Hemodynamic test in animal experiment

After anesthetized by intraperitoneal injection of 1% pentobarbital sodium (45 mg/kg; E602, Jiangsu Hengrui Pharmaceutical), the right external jugular vein was isolated, and polystyrene tubing (PE10, Smiths Medical, London, UK) was inserted into the right atrium and right ventricle. The mean right ventricular pressure (mRVP) was measured and recorded using a BL-420 F bioinformatics acquisition system (TechMan, Chengdu, China).

The rat neck's subcutaneous fascia and muscle layers were bluntly separated, and a ventilator catheter was connected to the trachea through an inverted "T"-shaped incision. A pulmonary artery catheter was inserted after opening the thoracic cavity of the rats, and the BL-420 F Biofunctional Information Acquisition System (TechMan, Chengdu, China) was connected to measure and record the mPAP.

Measurement of pulmonary vascular remodeling index in animal experiments

The experimental rats were euthanized via thoracotomy. The lungs and heart were rapidly removed from the chest cavity. The organs were washed with pre-cooled physiological saline, and the atrial tissues were trimmed. After blotting with filter paper, the free right ventricle (RV) and left ventricle plus septum (LV + S) were weighed separately. The right ventricular hypertrophy index (RVHI) was calculated as the RV to LV + S weight ratio.

Lung tissues fixed in 10% formaldehyde were taken transversely from the right pulmonary hilum for conventional paraffin embedding and stained with Hematoxylin and Eosin (HE). The prepared HE-stained sections were observed under a light microscope (XDS-1 A, Mitutoyo, Tokyo, Japan), and the small pulmonary arteries from different fields of view were randomly selected for imaging. Images were analyzed using ImageJ software (JEOL, Tokyo, Japan).

Staining of lung tissue and observation of mitochondrial morphology in experimental animals

After euthanized via thoracotomy, lung tissues (≤ 1 mm^3) were immediately dissected and fixed in 2.5% glutaraldehyde (A17876, Alfa Aesar, MA, USA) for 3–4 h. Following electron microscopy sample preparation, tissues were rinsed with 0.1 M phosphate buffer (pH 7.4) and then fixed in 1% osmium tetroxide in 0.1 M phosphate buffer (pH 7.4). Subsequently, tissues were dehydrated with a graded ethanol series. After embedding in resin and sectioning into ultrathin slices, the samples were stained with 3% uranyl acetate and lead citrate. Mitochondrial morphology and ultrastructural changes were observed and imaged using an HT7700 transmission electron microscope (HITACHI, Tokyo, Japan).

Table 1 The primers used in RT-qPCR

Primers	Sequences(5′-3′)
Mfn2(Rat)-F	TGAAGACACAGCACCTCAGCAATG
Mfn2(Rat)-R	GGTGTTCAGCAGGAGGTTGGAAG
IP3R3(Rat)-F	TCACCACCACGGAGCAGGAC
IP3R3(Rat)-R	TGCGGCGGGAGAACCAGTAG
Eif2α(Rat)-F	GCCAACACATACCTCGTTCCTCTG
Eif2α(Rat)-R	AAGCAGCACCAGCACCAGAAC
Drp1(Rat)-F	GAGAACTACCTTCCGCTGTATCGC
Drp1(Rat)-R	CACCATCTCCAATTCCACCACCTG
Opa1(Rat)-F	ATGCTCGCTATCACTGCCAACAC
Opa1(Rat)-R	CCTTCTTCTCGCCGTCTTCAGC
Bcl-2(Rat)-F	GAGAACTACCTTCCGCTGTATCGC
Bcl-2(Rat)-R	AGAGTGGCTGCTGCTGTTGTTAC
Perk(Rat)-F	CGCTGCTGCTGCTGTTCCTG
Perk(Rat)-R	AGCCAAATGCCGTATCCGATGTG
Atf4(Rat)-F	CTTAGAGGGCTACGGGACGGATG
Atf4(Rat)-R	CGTCAGCCTCGTGGTTGGTTC
Chop(Rat)-F	TGGCATCACCTCCTGTCTGTCTC
Chop(Rat)-R	CCCTCTCCTTTGGTCTACCCTCAG
Vdac1(Rat)-F	TCTGGTGCTTGGCTATGAGGGTTG
Vdac1(Rat)-R	GCGAGTGTTACTGTTTCCTGCGGT
SERCA(Rat)-F	ATCCTCTCCATCAAATCCACCACCC
SERCA(Rat)-R	TTGCCAATCTCAGTACTCACACCAG
GAPDH(Rat)-F	CTTCCGCTGATGCCCCCATGTTTGT
GAPDH(Rat)-R	CCAGTGGATGCAGGGATGATGTTCT

Culture and propagation of pulmonary artery smooth muscle cells in vitro

Purchased PASMCs were cultured in the smooth muscle cell culture medium containing Dulbecco's modified Eagle medium (DMEM) (11330057, Invitrogen, CA, USA) and 10% fetal bovine serum (FBS). Cells were incubated at 37℃ in a humidified incubator with 5% CO_2 and passaged using 0.25% trypsin-EDTA (Beyotime, China). PASMCs between passages 3 and 6 were used for further experiments. Cell proliferation was assessed using an MTT assay (M5655, Sigma, Darmstadt, Germany). Tumor necrosis factor-α (TNF-α) (AB9739, Abcam, Cambridge, UK) was used to stimulate PASMCs, and the optical density (OD) at specific time points was measured at 492 nm using a microplate reader.

Xestospongin C (Ab120914, Abcam) and cistanche phenylethanol glycosides (CPGs)(Changchun Medicinal Material Co, Changchun, China) were used to stimulate PASMCs. OD values were used to assess cell viability and determine the optimal concentration for intervention.

Reverse transcription-quantitative polymerase chain reaction (RT-qPCR)

Total RNA was isolated from lung tissues and PASMCs using TRNzol reagent (UN7E262I8, Invitrogen, CA, USA). mRNA was then reverse-transcribed into cDNA using the PrimeScript RT Reagent Kit (K1622, Zhennuobio, Shanghai, China). Primers for rat genes were designed and synthesized by Sangon Biotech (Shanghai, China). The RT-qPCR reactions were performed using SYBR® Premix Ex Taq™ II, ROX plus (P200601, Qiagen, Shanghai, China) in a Real-Time PCR system (Shanghai Sangon Biotechnology Co., Ltd.) at total 40 cycles for a total of 40 cycles (95 °C for 10 s for denaturation; 58 °C for 30 s for annealing; 60 °C for 10 s for extension). GAPDH was used as the internal reference, and the expression level of the target genes was calculated using the $2^{-\Delta\Delta Ct}$ method. The primer sequences used in this study are listed in Table 1.

Western blot analysis

Proteins were extracted using RIPA lysis buffer, separated on 10% SDS-PAGE gels, and transferred to polyvinylidene fluoride (PVDF) membranes (Millipore, USA). Primary antibodies against Mfn2 (1:1000; AB56889, Abcam, Cambridge, UK), IP3R3 (1:1000; AB125077, Abcam), optic atrophy 1 (Opa1) (1:1000; 612607, BD Biosciences, CA, USA), dynamin-related protein 1 (Drp1) (1:1000; 611112, BD Biosciences), B-cell lymphoma-2 (Bcl-2) (1:1000; 2870, Cell Signaling Technology, MA, USA), protein kinase R-like endoplasmic reticulum kinase (Perk) (1:1000; 3192, Cell Signaling Technology), C/EBP homologous protein (Chop) (1:1000; 2895, Cell Signaling Technology), eukaryotic initiation factor 2α (Eif2α)

(1:1000; 9722, Cell Signaling Technology), activating transcription factor 4 (Atf4) (1:1000; 11815, Cell Signaling Technology), voltage-dependent anion channel 1 (Vdac1) (1:1000; sc-390996, Santa Cruz Biotechnology, TX, USA), sarco/endoplasmic reticulum Ca^{2+} ATPase (SERCA) (1:1000; A11136, Thermo Fisher Scientific, MA, USA) and GAPDH (1:1000; 60004-1-lg, Proteintech, IL, USA) were used according to the manufacturer's protocols. Membranes were then incubated with secondary antibodies (anti-mouse, Abcam, Cambridge, UK, AB6789, 1:5000 dilution; anti-rabbit, Abcam, Cambridge, UK, AB205718,1:5000 dilution) at room temperature. Chemiluminescence was detected with Image Lab software (GE6100, Clinx, Shanghai, China) and quantified with Image J software.

Co-immunoprecipitation

According to the manufacturer's instructions, the co-immunoprecipitation (Co-IP) assay was performed using the Pierce Co-IP kit (Pierce, IL). A total of 100 μg of purified anti-IP3R3, anti-Mfn2, or anti-flag antibody was coupled to the resin. Protein samples (1 mg) were incubated with the antibody-coupled resin for 2 h. After mixing and washing, protein-antibody complexes were eluted in 50 μl of elution buffer. The eluted protein samples were then immunoblotted with the corresponding antibodies [17].

Construction of cell model with overexpressing/silencing Mfn2

Once the cells reached the logarithmic growth phase, they were seeded into 96-well plates at a density of 1.5×10^4 cells/well, incubated at 37 °C with 5% CO_2 for 24 h, and then transfected with viruses once the cell density reached 80-90%. The required amount of virus particles for PASMCs infection was calculated using MOI values for the Mfn2 overexpression virus and control virus (Genepharma Co., Ltd, Shanghai, China) at 12.5, 25, 50, 100, and 200, respectively. The MOI values for the Mfn2 silencing control virus (Genepharma Co., Ltd, Shanghai, China) were 2.5, 5, 10, 20, 40; for the Mfn2 silencing-521 virus, the MOI values were 5, 10, 20, 40, 80; and for the Mfn2 silencing-1176 virus and Mfn2 silencing-1302 virus, the MOI values were 12.5, 25, 50, 100, 200. Cells were infected with the virus for 72 h and then observed under a fluorescence microscope after 96 h. The optimal MOI value was determined based on a fluorescence ratio greater than 80-90% with minimal changes in cell morphology.

PASMCs were seeded in six-well culture plates to reach 90% confluence (approximately 1×10^5 cells/well) prior to transfection. Twenty-four hours before transfection, PASMCs were transfected with recombinant lentiviral Mfn2 gene expression and silencing plasmids (Shanghai GenePharma Co., Ltd.) at a multiplicity of infection (MOI) 100. LV3 fragments were used as cloning vectors, and the cloning sites were BamHI and EcoRI. The Mfn2 plasmid was synthesized and verified by the supplier to confirm the sequence accuracy. The lentiviral titer was maintained at 3×10^7 and used to transfect the Mfn2 overexpression and silencing plasmids into PASMCs, using a suspension of approximately 20,000 cells/μL.

Immunofluorescence staining to detect the expression of Mfn2

The expression of Mfn2 in PASMCs was detected using immunofluorescence staining. Paraffin-embedded slices were incubated with primary antibodies against Mfn2 (A12771, ABclonal, Shanghai, China) overnight at 4 °C. Subsequently, Cy3-conjugated goat anti-rabbit IgG antibody (1:200; SA00009-2, Proteintech, Wuhan, China) or FITC-conjugated goat anti-mouse IgG antibody (1:200; Ab6789, Abcam) was added, followed by a 1-hour incubation at room temperature. Fluorescence images were captured using confocal microscopy.

Measurement of the intracellular Ca^{2+} concentration

The concentrations of Ca^{2+} ions in the ER, cytoplasm, and mitochondria were measured using GENMED fluorescent detection kits (GMS10267.1 v.A, GMS10154 v.A, and GMS10153.1 v.A, Shanghai Jiemei Gene Pharmaceutical Technology Co., Ltd.). The experimental procedure was as follows: Cell samples were pretreated with 500 μL of GENMED cleaning solution (Reagent A), and then the solution was removed. Subsequently, 300 μL of fresh Reagent A was mixed with 30 μL of staining working solution and applied to the samples. For cytoplasmic Ca^{2+} detection, the samples were incubated in the dark at room temperature for 15 min. For ER and mitochondrial Ca^{2+} detection, samples were incubated in the dark at room temperature for 60 min. After incubation, the staining solution was removed, and the samples were washed with fresh Reagent A. Finally, the samples were covered with a coverslip and observed immediately under a confocal laser scanning microscope. Fluorescence signals were detected at excitation and emission wavelengths of 490/525 nm for ER Ca^{2+} ions, 350/405–420 nm for cytoplasmic Ca^{2+} ions, and 550/590 nm for mitochondrial Ca^{2+} ions.

CCK-8 detected cell activity

Cells were seeded in a 96-well plate at a density of 1×10^4 cells per well. PASMCs were treated according to the experimental groups. After incubation at 37 °C with 5% CO_2 for 24 h, 20 μl of CCK-8 solution was added to each well and incubated at 37 °C for another 4 hours. The absorbance of the treated cells at 450 nm was measured

using a microplate reader (Thermo MK3, USA) to determine cell viability.

Flow cytometry detection of apoptosis

PASMCs were digested with trypsin without EDTA and centrifuged at 1500 rpm for 5 min at room temperature. The cells were washed with PBS at 4 °C and centrifuged again at 1500 rpm for 5 min. The cells were then resuspended in 300 μL of 1× Binding Buffer. According to the manufacturer's instructions for the Annexin V-FITC/PI kit (401006, BestBio, Shanghai, China), 5 μL of Annexin V-FITC was added and mixed with the cells. The cell suspension was incubated in the dark at room temperature for 15 min. Subsequently, 10 μL of PI stain was added, and the cells were gently mixed and incubated in the dark at room temperature for 10 min. Flow cytometry was performed using a BD-FACSVerse flow cytometer (BD Biosciences, San Jose, USA), and data were analyzed with FlowJo 7.6 software (Tree Star, Oregon, USA).

Statistical analyses

All experiments were conducted in at least three biological replicates. Experimental personnel were blinded during both the experimental procedure and data analysis phases to minimize bias. Data are presented as mean ± SD unless otherwise indicated. For continuous variables, the normality of data was assessed using the Shapiro-Wilk test. After confirming normality, two group comparisons for means were performed using the Student's t-test, and multi-group comparisons were performed using one-way ANOVA followed by Tukey's post hoc test. For non-normally distributed data, two-group comparisons were performed using the Mann-Whitney U test, and multi-group comparisons were performed using the Kruskal–Wallis test, followed by Dunn's post hoc test. Analyses were performed using GraphPad Prism 9.5.1 (GraphPad Inc., La Jolla, CA, USA), with significance defined as $P < 0.05$.

During the data analysis phase, personnel responsible for statistical analysis were blinded to the experimental group assignments. Raw data were provided in a coded format, with group labels replaced by anonymized identifiers (e.g., Group A, Group B) by a third-party researcher. Blinding was maintained until all statistical tests were completed to prevent bias in data interpretation.

Results

The MCT-induced PAH rat model exhibits Endoplasmic reticulum stress and histopathological changes

The rat PAH model was successfully established via intraperitoneal injection of MCT (60 mg/kg). Hemodynamic assessments confirmed that mRVP, mPAP, and the right ventricular hypertrophy index (RVHI) were significantly elevated in the PAH rat model (Tables 2 and 3). RT-qPCR analysis indicated dysregulation of key ER stress-related genes, showing a significant reduction in Mfn2 expression and a marked increase in IP3R3, Perk, Eif2α, Chop, and Atf4 expression (Fig. 1A). Moreover, HE staining of lung tissues demonstrated prominent remodeling of the pulmonary vasculature, including thickening of the pulmonary artery vessel wall, lumen narrowing, disorganized tissue architecture with extensive inflammatory cell infiltration, and collagen fiber proliferation in the stroma (Fig. 1B). Transmission electron microscopy (TEM) analysis of PASMCs further revealed swollen mitochondria and disrupted cristae in PAH rats (Fig. 1C). These findings indicate significant ER stress activation and distinct histopathological changes, including cellular substructure disruption, in the lung tissues of MCT-induced PAH rats.

Table 2 Measurement results of hemodynamic parameters in different groups

Hemodynamic parameters	NC	PAH
mPAP(mmHg)	16.23 ± 3.98	49.76 ± 7.29$^{\#}$
mRVP(mmHg)	6.80 ± 2.16	29.57 ± 3.09$^{\#}$

Note The results showed that the mPAP and mRVP values of rats in the PAH group were higher than those of rats in the control group. **mPAP**: mean pulmonary artery pressure; **mRVP**: mean right ventricular pressure; **NC**: The normal control; **PAH**: MCT-induced PAH rats' model. Data are presented as mean ± SD. Data were analyzed using the Student's t-test (normal distribution) or Mann-Whitney U test (non-normal distribution). $^{\#}P < 0.01$, indicating a significant difference compared to the NC group

Table 3 Pulmonary vascular remodeling indicators in different groups

Indicators	NC	PAH
WT	28.45 ± 4.12	39.61 ± 19.80
ED	355.36 ± 22.64	160.05 ± 127.51
TA	284670.25 ± 96526.01	122325.35 ± 176570.55
IA	214215.50 ± 73550.06	70383.62 ± 113145.09
WT%	16.13 ± 3.22	58.47 ± 19.99*
WA%	24.92 ± 1.95	63.29 ± 19.34*
IA%	75.08 ± 1.95	36.71 ± 19.34*
RVHI	23.16 ± 1.63	37.95 ± 4.08*

Note The results showed an increase in small pulmonary artery vascular thickness, including a significant increase in WT%, WA%, and IA%, and an increase in the right ventricular hypertrophy index in the PAH group compared with the NC group. **NC**: The normal control; **PAH**: MCT-induced PAH rats' model; **WT**: wall thickness; **WA**: vascular wall area; **IA**: interstitial area; **TA**: total vascular area; **ED**: external diameter (the diameter of the external elasticplates); **WT%**=2×WT/ED×100%; **WA%**=(TA-IA)/TA×100%; **IA%**=IA/TA×100%; **RVHI**: right ventricular hypertrophy index. Data are presented as mean ± SD. Data were analyzed using the Student's t-test (normal distribution) or Mann-Whitney U test (non-normal distribution). $^{*}P < 0.05$, indicating a significant difference compared to the NC group

Development of a TNF-α-Induced PAH cell model in vitro to assess Mfn2 localization and interactions with ERS-related genes

TNF-α is a key inflammatory cytokine that promotes PASMCs proliferation during PAH development. Previous studies have confirmed that TNF-α can induce PAH cell models in vitro [18, 19]. Our study used varying

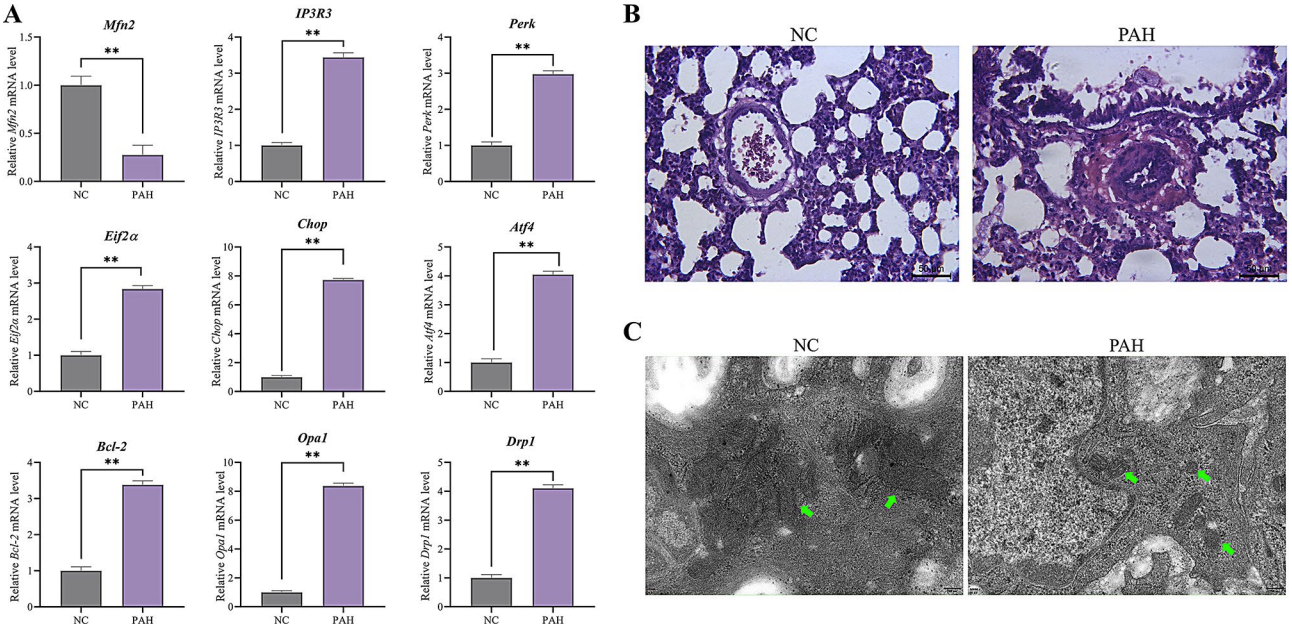

Fig. 1 The MCT-induced PAH rat model exhibits ERS and histopathological changes. **A**: The mRNA levels of key ER stress-related genes in lung tissue by RT-qPCR ($n=3$ per group). The results indicated dysregulation of ER stress-related genes, including a significant reduction in Mfn2 expression and a marked increase in IP3R3, Perk, Eif2α, Chop, and Atf4. **B**: HE staining of pulmonary arterioles (scale bar = 50 μm) showed that the walls of small pulmonary arteries were normal in the NC group, while they were significantly thickened in the lung tissues of PAH rats. **C**: TEM analysis of PASMCs mitochondrial structures between groups ($n=5$ to 6 images per group, scale bar = 200 nm). In the NC group, mitochondria were structurally intact, with preserved cristae and intact cell membranes. In the PAH group, mitochondria were shortened, and the membranes were damaged and disintegrated, with cristae ruptured or absent. Green arrows indicate mitochondria. NC: Normal control; PAH: MCT-induced PAH rat model. Data are presented as mean ± SD. Data were analyzed using the Student's t-test (normal distribution) or Mann-Whitney U test (non-normal distribution). $^{**}P<0.01$, indicating a significant difference compared to the NC group)

concentrations of TNF-α to stimulate primary PASMCs for 0, 12, 24, 36, 48, and 60 h to establish a PAH cell model. The results showed that TNF-α concentrations above 10 ng/mL significantly promoted PASMCs proliferation after 12 h of stimulation, with similar effects observed at 24, 36, 48, and 60 h. Based on these results, we determined that 12 h of TNF-α (20 ng/mL) was optimal for establishing the PAH cell model (Fig. 2A). Immunofluorescence staining further indicated that Mfn2 expression was primarily localized near the nucleus and mitochondria (Fig. 2B). Moreover, the Mfn2 expression level was significantly reduced in the TNF-α group compared to the NC group, consistent with our previous findings (Fig. 2C).

To further investigate the interactions between Mfn2 and ERS-related factors, we employed RNA interference (RNAi) to downregulate Mfn2 expression and observe changes in ERS-associated factors. Immunofluorescence staining showed that Mfn2 expression in the TNF-α-induced PAH cell model was significantly reduced compared to the control group, and overexpression of Mfn2 restored its expression. In contrast, silencing Mfn2 led to a further reduction in its expression. (Figure 2D and E).

To validate the efficiency of Mfn2 overexpression and silencing, we performed Western blot and RT-qPCR analyses. The results show that Mfn2 protein levels were significantly increased in the overexpression of Mfn2 and markedly reduced in siMfn2-treated cells (Fig. 2F and G). Consistently, RT-qPCR confirmed corresponding changes in Mfn2 mRNA levels (Fig. 2H). These data confirm the successful establishment of Mfn2 overexpression and silencing cell models, providing a reliable foundation for subsequent functional experiments. Additionally, RT-qPCR and western blotting confirmed that overexpression of Mfn2 decreased the expression of key ER stress-related factors, including IP3R3, Perk, Eif2α, Atf4, and Chop (Fig. 2I and K). Conversely, silencing Mfn2 increased the expression of these key ERS-related factors (Fig. 2L and N).

Mfn2 regulates Ca^{2+} homeostasis in PAH cells to maintain mitochondrial integrity

The ER is the primary intracellular Ca^{2+} reservoir, where transient Ca^{2+} ions are released into the cytosol and transferred to the mitochondria, facilitating cell signaling and ATP production [20, 21]. However, excessive Ca^{2+} release from the ER can lead to mitochondrial Ca^{2+} overload and cell death. Increased cytoplasmic Ca^{2+} concentration contributes to PASMCs over-proliferation in PAH [10, 22]. Using immunofluorescent probes in a PAH cell

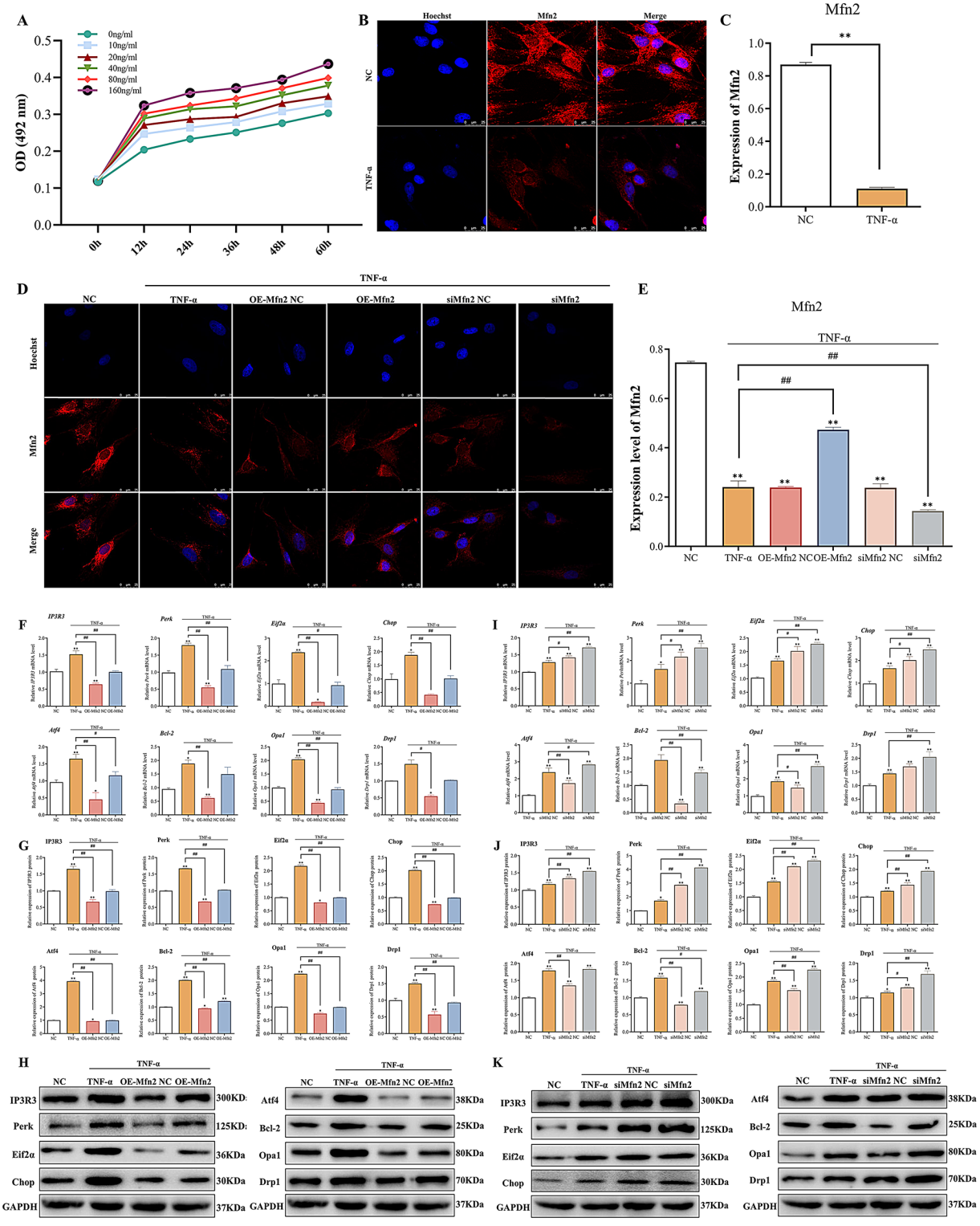

Fig. 2 (See legend on next page.)

(See figure on previous page.)

Fig. 2 Reduced Mfn2 expression and dysregulated ERS-related gene expression in the TNF-α-induced PAH cell model. **A**: Gradient concentrations of TNF-α stimulation in PASMCs over time. PASMCs were treated with varying concentrations of TNF-α (0-160 ng/mL) for 0, 12, 24, 36, 48, and 60 h, followed by an MTT assay to evaluate cell viability. The results showed that PASMCs proliferation significantly increased in response to TNF-α in a dose-dependent manner, which was more pronounced with extended incubation times. **B** and **C**: Immunofluorescence staining to observe Mfn2 in cellular substructures ($n = 3$ per group, scale bar = 25 μm). The immunofluorescence images showed a distinct red signal when Hoechst staining bound to Mfn2. Mfn2 expression was significantly lower in the TNF-α-induced PAH cell model compared to normal cells. Data were analyzed using the Student's t-test (normal distribution) or Mann-Whitney U test (non-normal distribution). **D** and **E**: Immunofluorescence staining was used to detect Mfn2 distribution and expression among different intervention groups ($n = 3$ per group, scale bar = 25 μm). The images showed that Mfn2 was expressed at lower levels in the TNF-α-induced PAH cell model compared to the normal control. Overexpression of Mfn2 restored its expression in the PAH cell model, whereas silencing Mfn2 further reduced its expression. **F**: The mRNA levels of key ER stress-related genes in PAH cells after Mfn2 overexpression were measured by RT-qPCR ($n = 3$ per group). **G and H**: Immunoblotting determined the protein levels of key ER stress-related genes in the PAH cell line after Mfn2 overexpression ($n = 3$ per group). **I**: The mRNA levels of key ER stress-related genes in the PAH cell model after Mfn2 silencing were measured by RT-qPCR ($n = 3$ per group). **J** and **K**: Immunoblotting determined the protein levels of key ER stress-related genes in the PAH cell model after Mfn2 silencing ($n = 3$ per group). The results showed upregulation of ER stress-related genes in the PAH cell model, including IP3R3, Perk, Eif2α, Atf4, Chop, Drp1, and Opa1. Silencing Mfn2 further increased the expression of these genes, while overexpression of Mfn2 decreased their expression. NC: Normal control; TNF-α: TNF-α-induced PAH cell model; OE-Mfn2 NC: Control for Mfn2 overexpression using an empty vector; OE-Mfn2: Overexpression of Mfn2 in the PAH cell model; siMfn2 NC: Control for Mfn2 silencing using an empty vector; siMfn2: Mfn2 silencing in the PAH cell model. Data are presented as mean ± SD. Data were analyzed by one-way ANOVA with Tukey's post hoc test (normal distribution) or Kruskal-Wallis test with Dunn's post hoc test (non-normal distribution). $^{*}P < 0.05$, significant compared to the NC group; $^{**}P < 0.01$, significant compared to the NC group; $\#P < 0.05$, significant compared to the PAH cell model; $\#\#P < 0.01$, significant compared to the PAH cell model

model, we found that Ca^{2+} concentrations in the cytoplasm and ER were significantly elevated in PAH cells, whereas mitochondrial Ca^{2+} concentrations were significantly reduced (Fig. 3A and B).

Interestingly, in addition to the previously identified regulated interactions between Mfn2 and IP3R3, we observed a significant increase in mitochondrial Ca^{2+} and a significant decrease in cytoplasmic Ca^{2+} in PAH cells with Mfn2 overexpression. In contrast, silencing Mfn2 expression resulted in elevated cytoplasmic Ca^{2+} and reduced mitochondrial Ca^{2+} concentrations (Fig. 3C and D). Furthermore, electron microscopy showed that mitochondria maintained intact morphology and structure with Mfn2 overexpression. In contrast, mitochondria in PAH cells with Mfn2 silencing exhibited pronounced swelling and cristae fragmentation (Fig. 3E). These findings suggest that the Mfn2-IP3R3 interaction is crucial for maintaining mitochondrial structural integrity and Ca^{2+} homeostasis in PAH cells.

Inhibition of IP3R3 and administration of cistanche phenylethanol glycosides (CPGs) reactivates the Mfn2-IP3R3 signaling

4-PBA is recognized as a typical ERS inhibitor, which assists in protein folding, increases protein stability, and reduces persistent UPR signaling. 4-PBA low molecular weight fatty acid, which prevents aggregation of misfolded proteins and attenuates ERS-mediated autophagy and apoptosis, has been used to treat excessive ERS [23]. Previous studies have shown that 4-PBA effectively inhibited key ERS factors, inhibited pulmonary vascular remodeling, and reduced pulmonary arterial pressure in monocrotaline-induced PAH rat model. The study demonstrated that Mfn2 expression levels were significantly reduced under PAH conditions. Notably, the 4-PBA intervention increased Mfn2 expression, suggesting its potential therapeutic role in alleviating PAH [24]. However, the specific regulatory mechanism of 4-PBA in PAH needs to be further investigated.

Mfn2 was confirmed to target and regulate IP3R3 expression, modulating ER stress and mitochondrial autophagy through their interplay, thereby inhibiting PASMCs proliferation and pulmonary vascular remodeling [9]. Based on our previous findings, we preliminarily conclude that there is a significant regulatory correlation between Mfn2 and IP3R3 expression. To further validate this interaction, we conducted a Co-IP analysis to confirm that Mfn2 interacts with IP3R3 in the PAH cell model (Fig. 4A). Under control conditions, a strong interaction between Mfn2 and IP3R3 was observed, as indicated by the robust co-immunoprecipitated band. However, treatment with TNF-α significantly reduced this interaction, as evidenced by the weakened intensity of the co-immunoprecipitated bands. This suggests that the TNF-α-induced PAH cell model disrupts the Mfn2-IP3R3 interaction. Interestingly, subsequent intervention with 4-PBA, an ER stress inhibitor, revealed that 4-PBA can modulate the Mfn2-IP3R3 signaling axis. To verify this observation, we further applied 4-PBA intervention in a PAH rat model in the following animal experiments.

It has been reported that cistanche phenylethanol glycosides (CPGs) [25], a traditional phytomedicinal extract, can play a crucial role in regulating inflammatory injury by reducing oxidative stress and inhibiting apoptotic pathways in reperfused myocardium [26]. Therefore, we hypothesized that CPGs may have a similar function in modulating inflammatory injury in PAH cells. Interestingly, after intervening in PAH cell models with the IP3R3 inhibitors Xestospongin C (XC) and CPGs, we observed increased expression of Mfn2 and sarco/endoplasmic reticulum Ca^{2+} ATPase (SERCA) compared to the TNF-α-induced PAH cell model. Conversely, IP3R3, Eif2α,

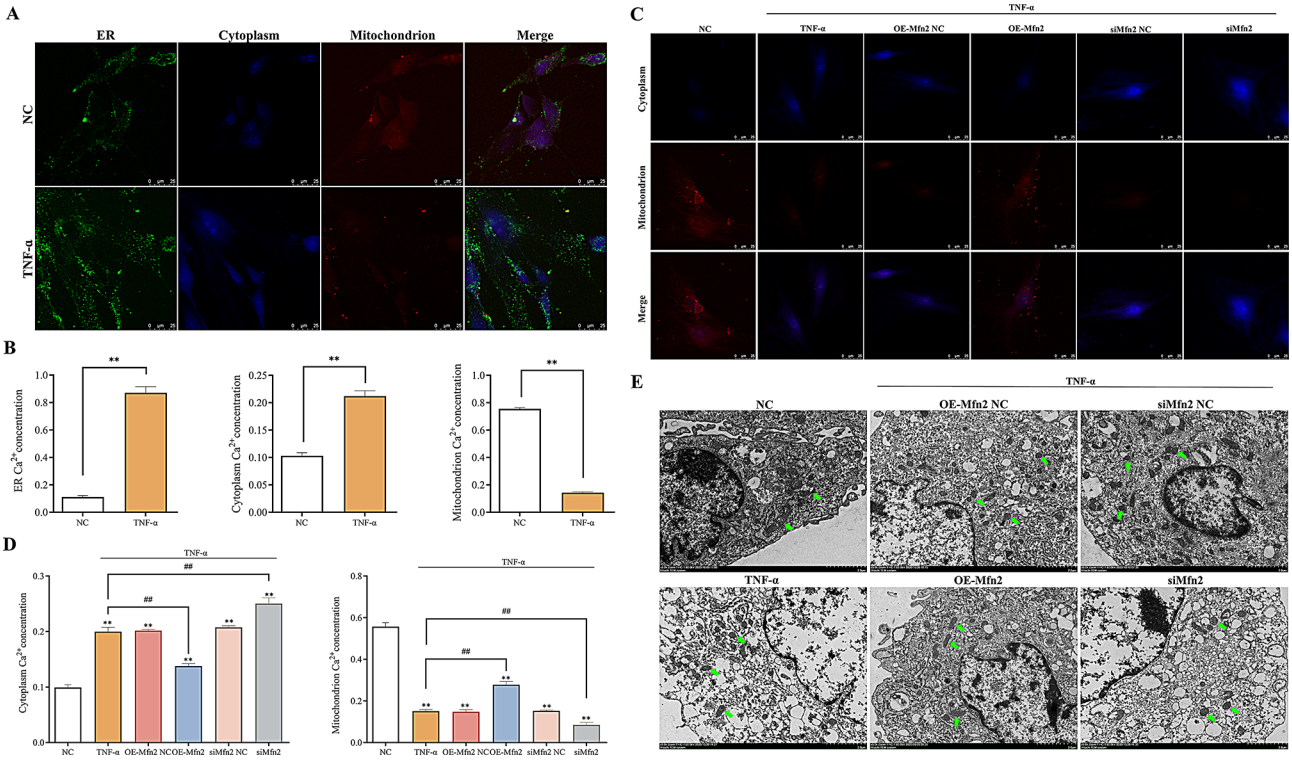

Fig. 3 Mfn2 regulates Ca^{2+} homeostasis in PAH cells to maintain mitochondrial integrity. **A** and **B**: Observed Ca^{2+} distribution in different cell substructures ($n = 3$ per group, scale bar = 25 μm). The results showed that Ca^{2+} concentrations were significantly higher in the cytoplasm and ER and lower in mitochondria in the PAH cell model compared to the normal control group. Data were analyzed using the Student's t-test (normal distribution) or Mann-Whitney U test (non-normal distribution). **C** and **D**: Ca^{2+} concentrations observed by immunofluorescence staining in different groups ($n = 3$ per group, scale bar = 25 μm). Ca^{2+} levels were measured in different cellular compartments, including the ER, cytoplasm, and mitochondria. The result indicated that overexpression of Mfn2 in the PAH cell model led to a significant decrease in cytoplasmic Ca^{2+} and a significant increase in mitochondrial Ca^{2+}. Conversely, silencing Mfn2 led to increased cytoplasmic Ca^{2+} and decreased mitochondrial Ca^{2+}. **E**: Detection of mitochondrial ultrastructure by TEM ($n = 5$ to 6 images or visual fields per group, scale bar = 2 μm). Green arrows indicate mitochondria. Electron microscopy showed that mitochondria were structurally intact with well-defined cristae in the normal control group. In contrast, mitochondria in the PAH cell model exhibited shortening, reduced numbers, swelling, and disrupted cristae, with some showing lysis and disappearance. Overexpression of Mfn2 restored mitochondrial structure, while silencing Mfn2 caused mitochondria to become smaller, with disrupted cristae and marked dissolution. ER: Ca^{2+} in the endoplasmic reticulum is green; Cytoplasm: Ca^{2+} in the cytoplasm is blue; Mitochondrion: Ca^{2+} in mitochondria is red. NC: Normal control; TNF-α: TNF-α-induced PAH cell model; OE-Mfn2 NC: Control for Mfn2 overexpression using an empty vector; OE-Mfn2: Overexpression of Mfn2 in the PAH cell model; siMfn2 NC: Control for Mfn2 silencing using an empty vector; siMfn2: Mfn2 silencing in the PAH cell model. Data are presented as mean ± SD. Data were analyzed by one-way ANOVA with Tukey's post hoc test (normal distribution) or Kruskal-Wallis test with Dunn's post hoc test (non-normal distribution). $^{**}P < 0.01$ indicates a significant difference compared to the NC group; $^{\#\#}P < 0.01$ indicates a significant difference compared to the TNF-α group

Chop, and Vdac1 expression was significantly reduced. Furthermore, inhibiting IP3R3 expression appeared to improve the feedback upregulation of Mfn2 expression, and this feedback mechanism was enhanced under Mfn2 overexpression conditions (Fig. 4B and D). Notably, across different intervention groups, we observed that the expression of Mfn2 could recover but not further inhibit IP3R3 expression after CPGs intervention, suggesting that CPGs likely function by directly restoring Mfn2 rather than inhibiting IP3R3. Additionally, SERCA, a gene involved in cellular Ca^{2+} homeostasis, was significantly restored following CPGs intervention. In contrast, Vdac1, a mitochondrial outer membrane Ca^{2+} regulator, and key ER stress genes Eif2α and Chop were significantly downregulated. These results support the hypothesis that the Mfn2-IP3R3 signaling maintains Ca^{2+} homeostasis in PAH cells by reducing ER stress.

Mfn2-IP3R3 signaling affects mitochondrial morphology and structure by regulating Ca^{2+} homeostasis in PAH cells via ER stress

Ca^{2+} concentrations in PAH cells were measured using immunofluorescence probes. The results indicated that the mitochondrial Ca^{2+} concentration in PAH cells significantly increased in the XC and CPGs intervention groups, whereas cytoplasmic Ca^{2+} concentration significantly decreased. These changes were more pronounced with Mfn2 overexpression (Fig. 5A and B). Transmission electron microscopy revealed mitochondrial membrane damage, cristae rupture, and autophagic vesicles

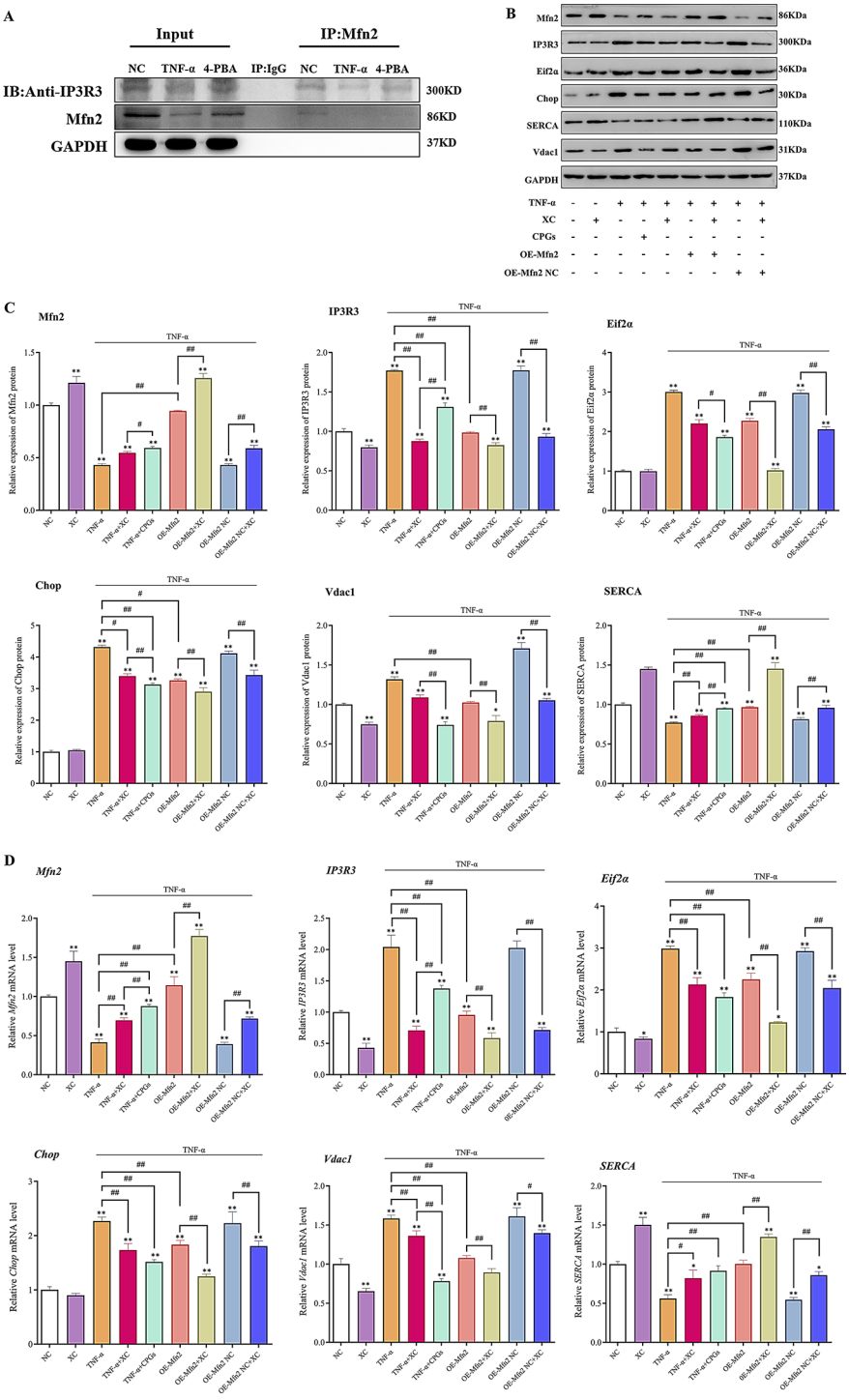

Fig. 4 (See legend on next page.)

(See figure on previous page.)

Fig. 4 Inhibition of IP3R3 and administration of CPGs reactivates the Mfn2-IP3R3 signaling. **A**: Immunoprecipitation (IP) analysis of the interaction between Mfn2 and IP3R3 showed that the expression of IP3R3 and Mfn2 was directly verified using antibodies in the Input group. In contrast, no expression of IP3R3 or Mfn2 was detected when IgG antibodies were used, excluding the possibility of non-specific protein binding. Furthermore, immunoprecipitation of IP3R3 with Mfn2 demonstrated co-precipitation of IP3R3 and Mfn2, indicating that IP3R3 and Mfn2 interact and are negatively regulated. **B** and **C**: Protein levels of key factors in PAH cells determined by immunoblotting ($n = 3$ per group). **D**: RT-qPCR measured the mRNA levels of key genes in PAH cells ($n = 3$ per group). IP3R3 expression was significantly increased in the PAH cell model, but interventions with the IP3R3 inhibitor XC, application of CPGs, and Mfn2 overexpression inhibited IP3R3 expression. The combination of Mfn2 overexpression and XC further reduced IP3R3 expression. Mfn2 expression was significantly decreased in the PAH cell model, but intervention with XC and CPGs promoted Mfn2 recovery, with CPGs showing a more pronounced effect. Additionally, the combination of Mfn2 overexpression and XC further increased Mfn2 expression, suggesting that IP3R3 inhibition can feedback upregulate Mfn2 expression. SERCA expression was decreased in the PAH cell model, but intervention with XC and CPGs indirectly increased SERCA expression. Overexpression of Mfn2 further enhanced SERCA expression, and combining XC with overexpression caused an additional increase, suggesting that the Mfn2-IP3R3 signaling may influence Ca^{2+} transport function in the ER. Vdac1 expression was significantly increased in the PAH cell model, and treatment with XC and CPGs reduced Vdac1 expression, with CPGs showing a more pronounced effect. Overexpression of Mfn2 significantly reduced Vdac1 expression, and combining XC further decreased it, indicating that the Mfn2-IP3R3 signaling may affect Ca^{2+} transport across the mitochondrial outer membrane. Eif2α and Chop were both upregulated in the PAH cell model. Treatment with XC or CPGs reduced Eif2α and Chop expression, with CPGs showing a stronger inhibitory effect. Moreover, overexpression of Mfn2 significantly reduced Eif2α and Chop expression, and further reduction was observed in combination with XC, suggesting that the Mfn2-IP3R3 signaling may affect the ERS process. NC: Normal control; TNF-α: TNF-α-induced PAH cell model; 4-PBA: TNF-α-induced PAH cell model treated with 4-PBA. XC: IP3R3 inhibitor Xestospongin C; CPGs: Cistanche phenylethanol glycosides; oe-Mfn2: Overexpression of Mfn2 in PAH cell model. Data are presented as the mean ± SD. Data were analyzed by one-way ANOVA with Tukey's post hoc test (normal distribution) or Kruskal-Wallis test with Dunn's post hoc test (non-normal distribution). $^{*}P < 0.05$, indicating a significant difference compared with NC. $^{**}P < 0.01$, indicating a significant difference compared with NC; $^{\#\#}P < 0.01$, indicating significant difference between groups

containing damaged mitochondrial fragments in the TNF-α-induced PAH cell model. However, with the intervention of the IP3R3 direct inhibitors, XC and CPGs preserved more intact cell membranes and mitochondrial structure, with minimal mitochondrial autophagy observed (Fig. 5C).

Mfn2-IP3R3 signaling regulates the phenotype of PAH cells in vitro

The overproliferation of PASMCs is a key factor in the pathogenesis of PAH. Our previous findings suggest that activation of Mfn2-IP3R3 signaling upregulates endoplasmic reticulum stress, subsequently altering Ca^{2+} distribution between the cytoplasm and mitochondria, ultimately compromising mitochondrial structural integrity and promoting mitochondrial autophagy. The CCK-8 and flow cytometry results demonstrated that blocking Mfn2-IP3R3 downstream signaling with the direct inhibitor XC, overexpressing Mfn2, or using CPGs significantly reduced the proliferative viability of PAH cells. Furthermore, CPGs exhibited a more pronounced inhibition of PAH cell proliferation. Overexpression of Mfn2 combined with IP3R3 inhibition produced greater inhibition of PAH cell proliferation compared to IP3R3 inhibition alone (Fig. 6A). Flow cytometry results also indicated that XC, CPGs, and Mfn2 overexpression all induced significant apoptosis in PAH cells. Additionally, CPGs induced more pronounced apoptosis than direct IP3R3 inhibition, while Mfn2 overexpression combined with Mfn2-IP3R3 inhibition led to more noticeable apoptosis in PAH cells (Fig. 6B and C).

Inhibition of ERS regulates Mfn2-IP3R3 signaling to balance Ca^{2+} homeostasis in mitochondria and maintain mitochondrial integrity

Our previous study demonstrated that 4-PBA could serve as a potent ERS inhibitor with an anti-PAH effect [9]. Thus, we aimed to determine whether interfering with ERS could inhibit PAH progression primarily by affecting the Ca^{2+} homeostasis mechanism regulated by Mfn2-IP3R3 signaling. Specifically, results from the PAH cell line showed that inhibiting ERS significantly increased Mfn2 expression while suppressing IP3R3 expression. Additionally, the expression of ERS-related genes, including Perk, Eif2α, Chop, and Atf4, was decreased in lung tissues of PAH rats treated with 4-PBA (Fig. 7A and C). These findings support our hypothesis that ERS activates aberrant Mfn2-IP3R3 signaling in mitochondria, disrupting Ca^{2+} homeostasis and inducing mitochondrial autophagy.

Further examination of cellular substructures confirmed that 4-PBA intervention significantly increased mitochondrial Ca^{2+} concentration while reducing cytoplasmic and ER Ca^{2+} levels in PAH cells (Fig. 7D and E). Furthermore, electron microscopy showed reduced mitochondrial swelling, cristae disruption, and diminished mitochondrial autophagy (Fig. 7G). PAH rats treated with 4-PBA exhibited significantly lower mRVP, mPAP, and RVHI levels (Tables 4 and 5). Histopathological analysis revealed notable recovery in right ventricular hypertrophy, pulmonary artery wall thickness, and arterial fibrosis in PAH rats (Fig. 7F).

Most importantly, we demonstrated that 4-PBA modulates the Mfn2-IP3R3 pathway by inhibiting ERS in PAH, thereby promoting and maintaining mitochondrial Ca^{2+} transport and homeostasis, protecting mitochondrial

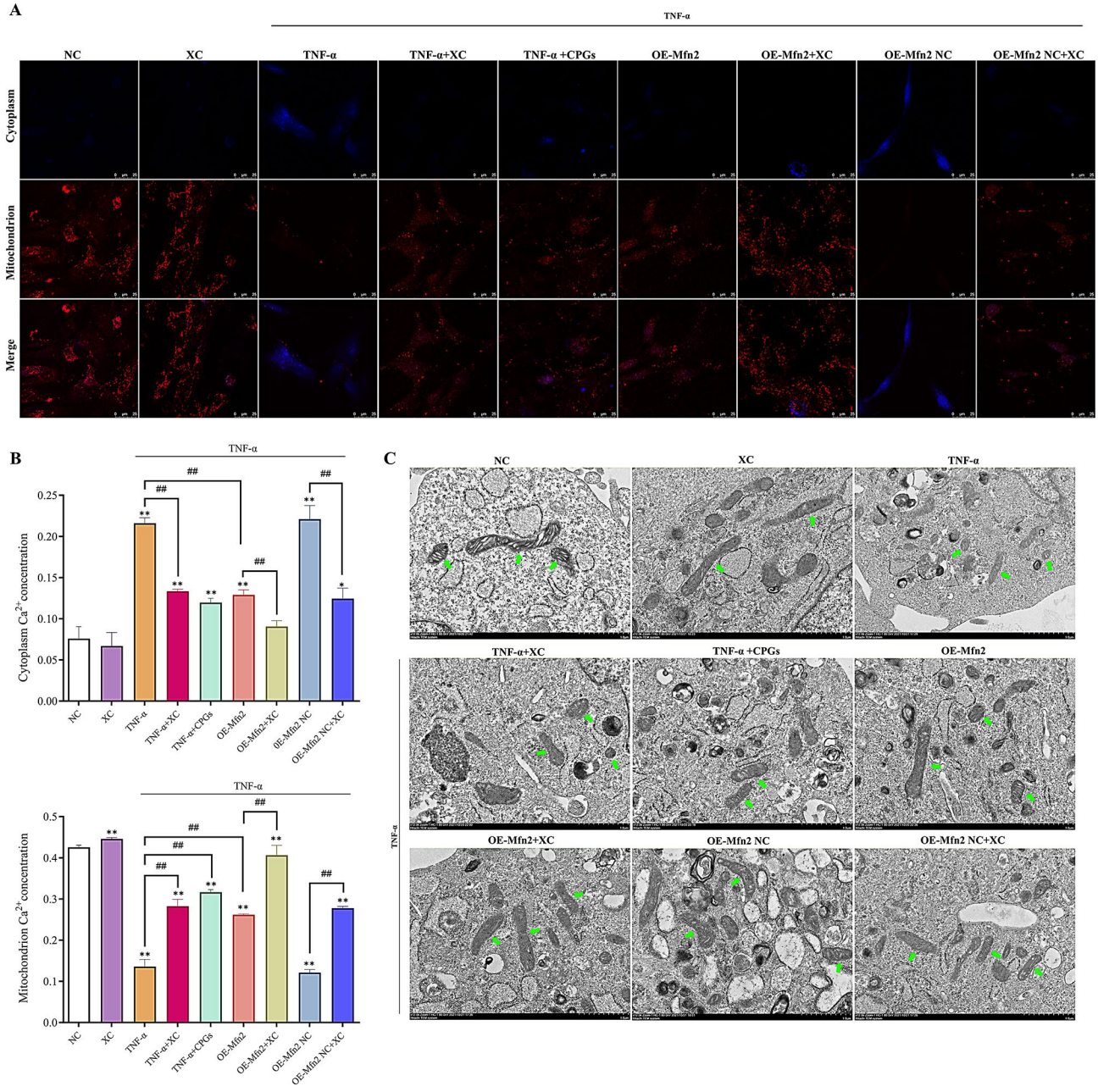

Fig. 5 Mfn2-IP3R3 signaling regulates Ca^{2+} homeostasis in PAH cells and influences mitochondrial morphology and structure. **A** and **B**: Ca^{2+} concentrations were observed by immunofluorescence staining in different groups ($n=3$ per group, scale bar = 25 μm). Cytoplasmic Ca^{2+} concentrations significantly increased in the PAH cell model, while mitochondrial Ca^{2+} concentrations significantly decreased. Treatment with the IP3R3 inhibitor XC, application of CPGs, or Mfn2 overexpression reversed these changes, reducing cytoplasmic Ca^{2+} concentrations and increasing mitochondrial Ca^{2+} concentrations. Mfn2 overexpression combined with XC had a more pronounced effect, suggesting that the Mfn2-IP3R3 signaling is crucial for regulating Ca^{2+} homeostasis in PAH cells. Furthermore, CPGs intervention had the most significant impact on restoring intracellular Ca^{2+} homeostasis. **C**: TEM observed mitochondrial ultrastructure ($n=5$ to 6 images or visual fields per group, scale bar = 1 μm). Green arrows indicate mitochondria. Data are presented as mean ± SD. Data were analyzed by one-way ANOVA with Tukey's post hoc test (normal distribution) or Kruskal-Wallis test with Dunn's post hoc test (non-normal distribution). $^{*}P<0.05$ indicates a significant difference compared with NC; $^{**}P<0.01$ indicates a significant difference compared with NC; $\#\#P<0.01$ indicates a significant difference between intervention groups

structural integrity, and ultimately playing a crucial role in PAH remodeling.

Discussion

The pathogenesis of pulmonary arterial hypertension (PAH) is complex, involving multiple pathological mechanisms such as intimal and media hypertrophy,

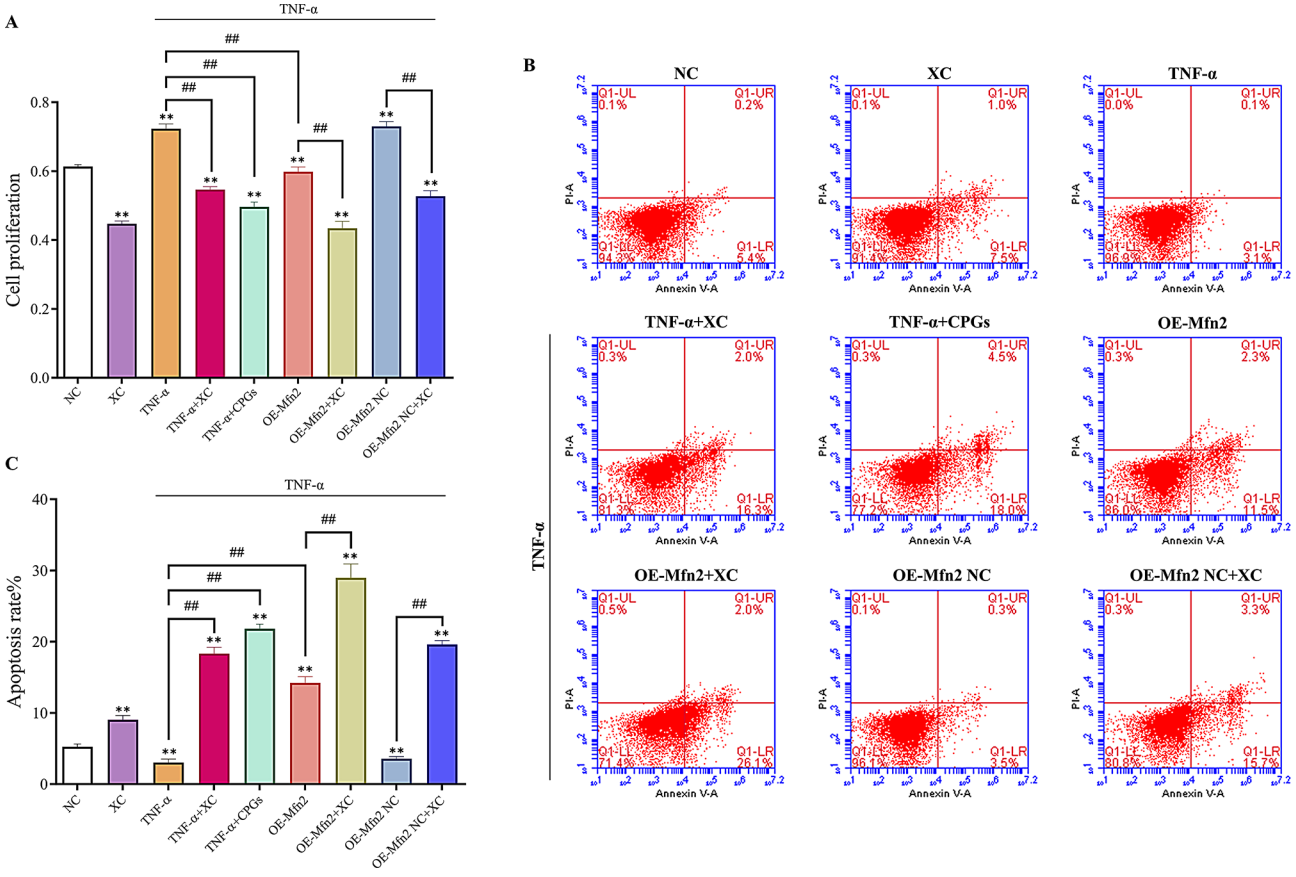

Fig. 6 Mfn2-IP3R3 signaling affects the proliferation and apoptosis of PAH cells. **A**: CCK-8 assay of cell proliferation in different intervention groups ($n=3$ per group). **B**: Flow cytometry analysis of apoptosis in different intervention groups ($n=3$ per group). Data are presented as mean ± SD. Data were analyzed by one-way ANOVA with Tukey's post hoc test (normal distribution) or Kruskal-Wallis test with Dunn's post hoc test (non-normal distribution). $^{**}P<0.01$ indicates a significant difference compared with NC; $\#\#P<0.01$ indicates a significant difference between intervention groups

small-vessel occlusion, stenosis, and plexus formation [27]. Studies have confirmed that the hyperproliferation of vascular cells primarily drives these pathological changes, with the proliferation of PASMCs being a hallmark of PAH, leading to vascular remodeling and occlusion of the pulmonary arteries [28]. Therefore, targeting the dysregulated proliferation and apoptosis of PASMCs and endothelial cells has been a key therapeutic strategy for PAH.

Increasing evidence indicates that ERS involves various PAH-triggering and PAH-promoting processes, such as inflammation, hypoxia, and gene mutations [29, 30]. Previous studies have demonstrated that ERS is significantly elevated in the MCT-induced PAH rat model, mainly characterized by upregulation of PERK, ATF6, and IRE1 signaling pathways [31]. As a chemical chaperone, 4-PBA has been shown to inhibit ERS and reverse pulmonary arterial remodeling. However, its specific molecular mechanism remains elucidated.

Previous evidence suggests that Mfn2 is a key mitochondrial fusion protein that connects the ER-mitochondria tethering, maintaining Ca^{2+} homeostasis and glucose metabolism [32]. Our study confirmed that the lung tissue from MCT-induced PAH rats exhibited significant pathological features, including pulmonary vascular remodeling and right ventricular hypertrophy. Furthermore, our findings elucidate the biological function of Mfn2 and propose a novel molecular mechanism: ERS activation in MCT-induced PAH rats mediates the downregulation of Mfn2 expression and the upregulation of IP3R3 expression, whereas inhibiting ERS yields the opposite effect. Additionally, we found that ER-induced Mfn2-IP3R3 signaling could induce mitochondrial autophagy, potentially serving as a critical mechanism that triggers PAH development. Inhibition of ER activation successfully reversed mitochondrial autophagy in PAH cells, improved pulmonary hemodynamics, and reduced vascular remodeling in PAH rats. Therefore, our study identifies a key pathway through which ER activation induces mitochondrial autophagy and contributes to understanding the molecular mechanisms underlying PAH pathogenesis.

IP3R3, a member of the IP3R family, forms Ca^{2+} channels in the ER and plays a crucial role in intracellular

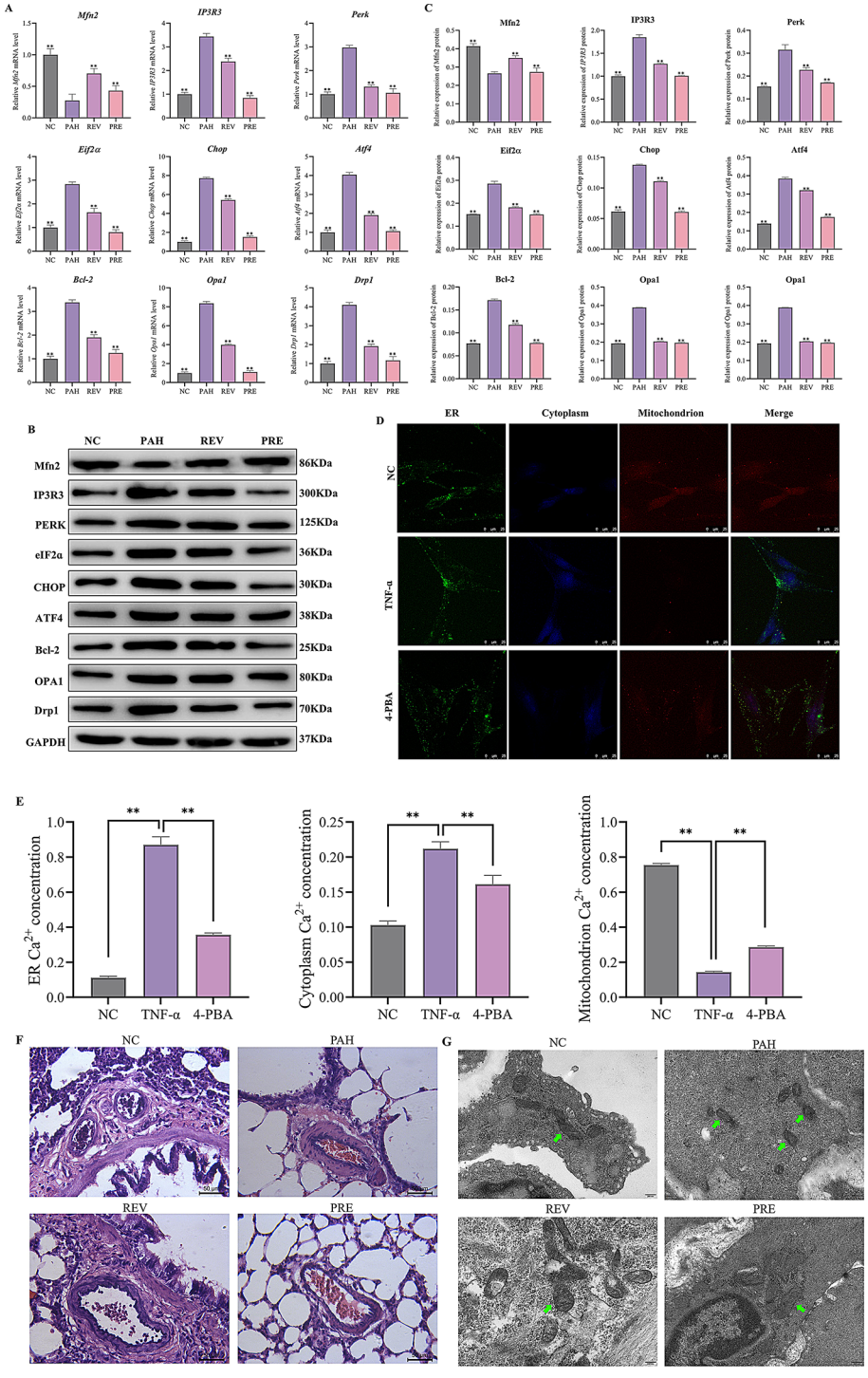

Fig. 7 (See legend on next page.)

(See figure on previous page.)

Fig. 7 Inhibition of ERS regulates Mfn2-IP3R3 signaling to balance Ca^{2+} homeostasis in mitochondria and thereby maintain mitochondrial integrity. **A**: RT-qPCR determined the mRNA levels of key genes in lung tissue ($n=3$ per group). **B** and **C**: Protein levels of key genes in lung tissue determined by immunoblotting ($n=3$ per group). NC: Normal control group; PAH: Model group; REV (Remediation group): Saline administered daily at 500 mg/(kg·d) on the first day, followed by 4-PBA at 500 mg/(kg·d) for 2 weeks; PRE (Prevention group): Rats were given 4-PBA at 500 mg/(kg·d) daily for 4 weeks from the start. $^{**}P<0.01$, indicating a significant difference compared to the PAH group. **D** and **E**: Ca^{2+} concentration observed by immunofluorescence staining in different groups ($n=3$ per group). ER: Ca^{2+} in endoplasmic reticulum marked in green; Cytoplasm: Ca^{2+} in cytoplasm marked in blue; Mitochondrion: Ca^{2+} in mitochondria shown in red. NC: Normal control; TNF-α: TNF-α-induced PAH cell model; 4-PBA: 4-PBA intervention group. **F**: Mitochondrial ultrastructure observed by TEM in lung tissue of MCT-induced PAH rats ($n=5$ to 6 images or fields per group, scale bar = 200 nm). The results indicated that 4-PBA restored mitochondrial morphology, showing clear cristae structure and reduced mitochondrial autophagy. Green arrows indicate mitochondria. **G**: HE staining of pulmonary arterioles (scale bar = 50 μm). HE staining of lung tissue showed thinner arterial walls and reduced inflammatory infiltration in the 4-PBA intervention groups (REV, PRE) compared to the PAH group. Data are presented as mean ± SD. Data were analyzed by one-way ANOVA with Tukey's post hoc test (normal distribution) or Kruskal-Wallis test with Dunn's post hoc test (non-normal distribution). $^{**}P<0.01$ indicates a significant difference compared with PAH or TNF-α

Ca^{2+} homeostasis and regulating apoptosis [33]. IP3R3 is localized at the mitochondria-associated ER membrane, serving as a crucial signaling platform that not only induces intracellular Ca^{2+} overload but also reduces mitochondrial Ca^{2+} uptake. This mechanism highlights the significance of altered mitochondrial dynamics in PAH pathogenesis [34–36]. Notably, we confirmed the interaction between Mfn2 and IP3R3 using Co-IP in PAH cells. We observed a feedback increase in Mfn2 expression following treatment with the IP3R3 inhibitor Xestospongin C. Studies indicate that Mfn2 and IP3R3 are both vital proteins that regulate various aspects of cellular function, particularly mitochondrial dynamics, Ca^{2+} signaling, and ER function. Their interactions are part of the intricate communication network between the ER and mitochondria. Mfn2 has been reported to influence ER-mitochondrial connections, as well as the structure and function of the ER, while IP3R3 releases Ca^{2+} into the cytoplasm, regulating processes such as cell signaling, muscle contraction, and apoptosis. Regarding the regulatory relationship between Mfn2 and IP3R3, our research demonstrates that their synergistic roles in ER-mitochondrial communication are essential for maintaining cellular function and managing PAH-induced cellular stress. Furthermore, these regulators may exert indirect effects via cellular signaling pathways or at the ER-mitochondrial interface, contributing to cellular homeostasis, including mitochondrial dynamics and Ca^{2+} signaling. However, the complex relationship between Mfn2 and IP3R3 still lacks definitive evidence for their regulatory mechanisms. It is possible that they also have independent roles within their respective organelles, participating in distinct aspects of cellular function.

Table 4 Measurement results of hemodynamic parameters in different groups

Hemodynamic parameters	NC	PAH	REV	PRE
mPAP(mmHg)	14.51 ± 2.58	55.57 ± 12.83*	32.90 ± 3.72$^{\#}$	22.34 ± 1.21$^{\#}$
mRVP(mmHg)	7.90 ± 0.72	33.16 ± 7.02*	20.87 ± 2.80$^{\#}$	17.24 ± 1.59$^{\#}$

Note **mPAP**: mean pulmonary artery pressure; **mRVP**: mean right ventricular pressure; **NC**: normal control group; **PAH**: model group; **REV(Remediation group)**: Saline was administered daily at a dose of 500 mg/(kg-d) on the first day of the experiment, and then 4-PBA suspension was administered to rats at a dose of 500 mg/(kg-d) for 2 weeks; **PRE(Prevention group)**: Rats were administered 4-PBA suspension at a dose of 500 mg/(kg-d) daily for 4 weeks starting on the first day of the experiment. Data are presented as the mean ± SD. Data were analyzed by one-way ANOVA with Tukey's post hoc test (normal distribution) or Kruskal-Wallis test with Dunn's post hoc test (non-normal distribution). $^{*}P<0.05$ compared with the NC group. $^{\#}P<0.05$ compared with the PAH group

Table 5 Changes in pulmonary vascular remodeling-related indicators in different groups

	NC	PAH	REV	PRE
WT	27.91 ± 3.72	45.30 ± 29.20	48.09 ± 9.02	45.54 ± 11.55
ED	323.59 ± 41.47	248.38 ± 196.09	480.87 ± 207.75	455.88 ± 182.29
TA	264578.25 ± 84165.12	251434.84 ± 271156.31	427548.50 ± 139171.59	394318.00 ± 93711.46
IA	188974.00 ± 70013.31	162010.08 ± 197912.11	305960.75 ± 131797.41	282668.88 ± 86043.81
WT%	17.52 ± 3.36	47.60 ± 18.97*	25.42 ± 15.24$^{\#}$	22.38 ± 8.98$^{\#}$
WA%	29.50 ± 6.06	52.03 ± 20.65*	31.89 ± 12.75$^{\#}$	29.74 ± 8.99$^{\#}$
IA%	70.50 ± 6.06	47.97 ± 20.65*	68.11 ± 12.75$^{\#}$	70.26 ± 8.99$^{\#}$
RVHI	22.85 ± 1.60	40.24 ± 4.54*	29.83 ± 5.07$^{\#}$	24.98 ± 2.49$^{\#}$

Note The results showed an increase in small pulmonary artery vascular thickness, including a significant increase in WT%, WA%, and IA%, and an increase in the right ventricular hypertrophy index in the PAH group compared with the NC group. **NC**: The normal control; **PAH**: MCT-induced PAH rats' model; **REV(Remediation group)**: Saline was administered daily at a dose of 500 mg/(kg-d) on the first day of the experiment, and then the 4-PBA suspension was administered to rats at a dose of 500 mg/(kg-d) for 2 weeks; **PRE(Prevention group)**: Rats were administered 4-PBA suspension at a dose of 500 mg/(kg-d) daily for 4 weeks starting on the first day of the experiment. WT: wall thickness; WA: vascular wall area; IA: interstitial area; TA: total vascular area; ED: external diameter (the diameter of the external elasticplates); WT%=2×WT/ED×100%; **WA%**=(TA-IA)/TA×100%; I**A%**=IA/TA×100%; RVHI: right ventricular hypertrophy index. Data are presented as the mean ± SD. Data were analyzed by one-way ANOVA with Tukey's post hoc test (normal distribution) or Kruskal-Wallis test with Dunn's post hoc test (non-normal distribution). $^{*}P<0.05$ compared with NC group; $^{\#}P<0.05$ compared with PAH group

It is also important to consider several factors regarding this interaction. Firstly, the interaction between Mfn2 and IP3R3 may be influenced by various regulatory factors, including the cellular microenvironment, post-translational modifications, and competition with other binding proteins. Even when interactions are present, the strength of these associations can be modulated by phosphorylation events and competing interactions [37]. Besides, Mfn2 is primarily localized to the outer mitochondrial membrane, whereas IP3R3 is restricted to the endoplasmic reticulum membrane; this difference in subcellular localization may be influenced by mitochondria-endoplasmic reticulum contacts (MERCs) [38]. Moreover, the technical challenges inherent in Co-IP may affect protein interaction detection [39, 40].

The regulatory relationship between Mfn2 and IP3R3 is critical for maintaining intracellular Ca^{2+} homeostasis. Ca^{2+} serves as an essential signaling molecule that supports numerous cellular processes. During the pathophysiological progression of PAH, disrupted Ca^{2+} homeostasis may result in abnormal proliferation of pulmonary artery endothelial cells, inflammation, and vasoconstriction. Abnormal Mfn2 and IP3R3 function can lead to endoplasmic reticulum stress and mitochondrial dysfunction, further disrupting Ca^{2+} homeostasis, exacerbating the abnormal growth and constriction of the pulmonary vasculature, and promoting inflammation. Despite promising findings, research in this area remains exploratory, and further studies are required to elucidate the precise relationship between these regulators and PAH. In our study, we employed an ER stress inhibitor, 4-PBA, and a novel herbal component, CPGs, and observed that both significantly reversed pathological processes in PAH cell models and PAH rats under different intervention conditions.

Previous studies have reported that 4-PBA, as a chemical chaperone, inhibits endoplasmic reticulum stress by stabilizing peptide structure and enhancing the folding capacity of the ER lumen [41]. This reduces cellular inflammatory response, oxidative stress, ER stress, and apoptosis, demonstrating significant protective effects in cardiovascular, neurological, and metabolic diseases [42–44]. In our study, 4-PBA significantly reduced mPAP and reversed right ventricular remodeling in MCT-induced PAH rats. Mechanistic analysis revealed that 4-PBA significantly reduced key markers of ER stress, such as Perk, Eif2α, Chop, and Atf4. Additionally, 4-PBA increased mitochondrial Ca^{2+} concentration by regulating the Mfn2-IP3R3 signaling axis, thereby protecting mitochondrial morphology, reducing mitochondrial autophagy, and ultimately blocking PAH progression. Furthermore, we confirmed that cistanche phenylethanol glycosides (CPGs), a novel active compound from Traditional Chinese Medicine (TCM), also had a significant therapeutic effect on PAH. CPGs restored Mfn2 expression in the PAH cell model while inhibiting IP3R3 expression. CPGs also significantly reduced the expression of ERS regulators, including Eif2α and Chop, downregulated the mitochondrial outer membrane Ca^{2+} regulator Vdac1, and restored the intracellular Ca^{2+} homeostasis regulator SERCA.

Recent studies have confirmed that SERCA is a crucial membrane protein located on the ER membrane, which plays a key role in reducing intracellular Ca^{2+} levels by transporting free Ca^{2+} back into the ER lumen [45]. Voltage-dependent anion channel 1 (Vdac1) is a protein channel on the outer mitochondrial membrane that primarily regulates ion permeability and the exchange of substances between the mitochondria and cytoplasm [46]. Our study observed an imbalance in Ca^{2+} homeostasis in PAH cells, characterized by a significant increase in mitochondrial Ca^{2+} concentration and a significant decrease in cytoplasmic Ca^{2+} concentration. CPGs intervention effectively regulated Ca^{2+} distribution in PAH cells, promoted mitochondrial morphological and structural repair, and inhibited cell proliferation. These findings suggest that CPGs may directly target the Mfn2-IP3R3 signaling axis, reduce ERS, maintain Ca^{2+} homeostasis and mitochondrial integrity in PAH cells, inhibit PASMCs proliferation, and ultimately exert an anti-PAH effect.

Ryanodine receptors (RyRs) are large cation-selective ligand-gated channels expressed on the sarcoplasmic reticulum (SR) membrane, mediating the controlled release of Ca^{2+} from the SR and playing crucial roles in numerous cellular processes. RyRs are primarily expressed on the ER or SR membranes in muscle cells, mediating Ca^{2+} release from ER/SR stores [47, 48]. Mammals express three isoforms of RyRs (RyR1, RyR2, and RyR3), which share 63–67% sequence identity [49, 50]. Dysregulated Ca^{2+} handling, particularly aberrant SR Ca^{2+} leakage, is a key pathophysiological mechanism underlying various cardiac disorders, including heart failure (HF), atrial fibrillation, catecholaminergic polymorphic ventricular tachycardia (CPVT), and other arrhythmias [51–54]. In pulmonary arterial hypertension (PAH), Ca^{2+} release from the SR via RyRs is a major contributor to elevated Ca^{2+} in PASMCs, with all three RyR isoforms (RyR1, RyR2, and RyR3) expressed in these cells. RyR2-mediated Ca^{2+} release is significant in hypoxia-induced contraction and remodeling [55, 56]. While RyRs and IP3Rs exhibit distinct physiological and pharmacological properties, their functions are interconnected. Localized Ca^{2+} signals, termed Ca^{2+} "sparks" and "puffs", generated by RyR and IP3R clusters, respectively, can propagate to neighboring receptors, triggering global Ca^{2+} waves and oscillations that mediate neuronal excitability and synaptic plasticity [57]. Evidence shows that

intracellular Ca^{2+} release channels can cooperate, creating positive feedback during activation. Specifically, agonist-dependent activation of IP3Rs can promote RyR activation, amplifying and shaping the resulting Ca^{2+} signal. Although direct evidence for the mechanism behind this interaction is limited, it likely involves some form of Ca^{2+}-induced Ca^{2+} release in response to local Ca^{2+} increases [58]. While our study primarily focuses on the Mfn2-IP3R3 signaling pathway, the role of RyRs in intracellular Ca^{2+} regulation and PAH pathogenesis is well-established. Future studies could explore the interplay between RyRs and Mfn2-IP3R3 signaling to provide a more comprehensive understanding of Ca^{2+} homeostasis in PAH.

The pathogenesis of PAH is complex, and the Mfn2-IP3R3 interaction forms part of the intricate communication between the ER and mitochondria. However, the molecular mechanism underlying this regulatory relationship remains unclear. Our study confirms the presence of an Mfn2-IP3R3 relationship, demonstrating that increased Mfn2 expression leads to reduced IP3R3 expression, while decreased IP3R3 expression provides feedback to upregulate Mfn2. Moreover, we further confirmed that modulation of the Mfn2-IP3R3 signaling axis can reduce ERS, playing a crucial role in maintaining Ca^{2+} homeostasis, preserving mitochondrial structure, and inhibiting PASMCs proliferation in PAH. Additionally, we found that both 4-PBA and CPGs could regulate the Mfn2-IP3R3 signaling axis, which is critical for inhibiting PAH progression. However, further multi-omics studies are needed to elucidate the pathogenesis of PAH involving mitochondria, ER, and MAMs, particularly to identify key factors of Ca^{2+}-regulated signaling in MAMs and their regulatory networks.

This study had several limitations. Due to the lack of human PAH tissue and cell samples, current research only focuses on animal models. It is necessary to investigate the Mfn2-IP3R3 signaling axis in samples obtained from PAH patients further. Additionally, although we observed the regulatory role of the Mfn2-IP3R3 signaling axis in PAH, its upstream regulatory factors and downstream effector pathways remain unclear. Future studies will integrate multi-omics and CRISPR screening technologies to systematically analyze the molecular network of this pathway. Despite these limitations, we consider that our findings have revealed a promising opportunity to develop novel therapeutic interventions for PAH by targeting the Mfn2-IP3R3 signaling axis.

Conclusion

Our study confirmed that the regulatory relationship between Mfn2 and IP3R3 plays a crucial role in the pathogenesis of PAH, involving key molecular mechanisms of intracellular Ca^{2+} homeostasis and maintaining mitochondrial morphology and structure. Furthermore, we demonstrated that 4-PBA and CPGs modulate the Mfn2-IP3R3 interaction to enhance mitochondrial Ca^{2+} levels, thereby maintaining Ca^{2+} homeostasis, preserving mitochondrial integrity, and restoring pulmonary artery smooth muscle cell function, resulting in reducing cellular stress and inhibiting PAH progression. The findings of this study provide a new perspective for developing PAH-targeted therapeutic drugs and a necessary theoretical basis for utilizing TCM in the prevention and treatment of PAH.

Acknowledgements
We want to thank Jian-hua Yang, director of the Pharmacy department at the First Affiliated Hospital of Xinjiang Medical University in Urumqi, China, for providing crucial assistance in the pharmacology research projects.

Author contributions
RW, JW, and YW conceived and designed the research. RW, JW, JY, ZL, MZ, YC, FL, DJ, and JG performed the experiments and analyzed the data. XL and YW were responsible for all aspects of this study's integrity, including the resources, writing, review, editing, supervision, project management, and funding acquisition. All authors examined and approved the final draft before it was submitted.

Funding
This work was supported by the Xinjiang Uygur Autonomous Region Youth Science and Technology Top Talent Project-Youth Science and Technology Innovation Talent Training (No.2022TSYCCX0034), the National Natural Science Foundation of China (No.82260081).

Data availability
All data used for the research are described in the article. Data will be available upon request from the corresponding author.

Declarations

Ethical approval and consent to participate
The hospital's Institutional Animal Care and Use Committee approved all animal experiments before the study began (*approval number: IACUC20190416-01*). Additionally, we ensure that animal ethical requirements are followed during animal research, including determination of the purpose of the experiment and assessing its necessity, animal house practices, animal experimentation skills, routine husbandry and care, and euthanasia.

Consent for publication
Not applicable.

Competing interests
The authors declare that they have no competing interests.

Author details
[1]Department of General Medicine, First Affiliated Hospital of Xinjiang Medical University, Urumqi 830011, China
[2]Department of Pharmacy, First Affiliated Hospital of Xinjiang Medical University, Urumqi 830011, China
[3]College of Pharmacy, Xinjiang Medical University, Urumqi 830011, China
[4]Animal Laboratory Center, Xinjiang Medical University, Urumqi 830011, China
[5]Electron Microscope Lab, Xinjiang Medical University, Urumqi 830011, China
[6]Department of General Surgery, Lingcheng District People's Hospital, Dezhou 253500, China
[7]A State Key Laboratory of Pathogenesis, Prevention and Treatment of High Incidence Diseases in Central Asia, Clinical Medical Research Institute, First Affiliated Hospital of Xinjiang Medical University, Urumqi 830011, China

[8]Department of Cardiology, First Affiliated Hospital of Xinjiang Medical University, Urumqi 830011, China

Received: 31 May 2024 / Accepted: 14 March 2025
Published online: 24 March 2025

References

1. Ruopp NF, Cockrill BA. Diagnosis and treatment of pulmonary arterial hypertension: A review. JAMA. 2022;327:1379–91.
2. Simonneau G, Montani D, Celermajer DS, Denton CP, Gatzoulis MA, Krowka M, Williams PG, Souza R. Haemodynamic definitions and updated clinical classification of pulmonary hypertension. Eur Respir J. 2019;53:1801913.
3. Gallardo-Vara E, Ntokou A, Dave JM, Jovin DG, Saddouk FZ, Greif DM. Vascular pathobiology of pulmonary hypertension. J Heart Lung Transpl. 2023;42:544–52.
4. Cullivan S, Lennon D, Meghani S, Minnock C, McCullagh B, Gaine S. Incidence and outcomes of pulmonary hypertension in the Ireland. BMJ Open Respir Res. 2022;9:e001272.
5. Rocha AG, Franco A, Krezel AM, Rumsey JM, Alberti JM, Knight WC, Biris N, Zacharioudakis E, Janetka JW, Baloh RH, et al. MFN2 agonists reverse mitochondrial defects in preclinical models of Charcot-Marie-Tooth disease type 2A. Science. 2018;360:336–41.
6. Song Z, Song H, Liu D, Yan B, Wang D, Zhang Y, Zhao X, Tian X, Yan C, Han Y. Overexpression of MFN2 alleviates sorafenib-induced cardiomyocyte necroptosis via the MAM-CaMKIIδ pathway in vitro and in vivo. Theranostics. 2022;12:1267–85.
7. Chen IC, Liu YC, Wu YH, Lo SH, Wang SC, Li CY, Dai ZK, Hsu JH, Yeh CY, Tseng YH. Proteasome inhibitors decrease the viability of pulmonary arterial smooth muscle cells by restoring Mitofusin-2 expression under hypoxic conditions. Biomedicines. 2022;10:873.
8. Ryan JJ, Marsboom G, Fang YH, Toth PT, Morrow E, Luo N, Piao L, Hong Z, Ericson K, Zhang HJ, et al. PGC1α-mediated mitofusin-2 deficiency in female rats and humans with pulmonary arterial hypertension. Am J Respir Crit Care Med. 2013;187:865–78.
9. Wu Y, Yan Q, Wang J, Zhang M, Wang R, Wang S. Effect of Endoplasmic reticulum stress-mitochondrial autophagy pathway on pulmonary hypertension in rats. Chin J Comp Med. 2022;32:53–9.
10. Masson B, Montani D, Humbert M, Capuano V, Antigny F. Role of Store-Operated Ca(2+) entry in the pulmonary vascular remodeling occurring in pulmonary arterial hypertension. Biomolecules. 2021;11:1781.
11. Santos-Gomes J, Le Ribeuz H, Brás-Silva C, Antigny F, Adão R. Role of ion channel remodeling in endothelial dysfunction induced by pulmonary arterial hypertension. Biomolecules. 2022;12:484.
12. Shibata A, Uchida K, Kodo K, Miyauchi T, Mikoshiba K, Takahashi T, Yamagishi H. Type 2 inositol 1,4,5-trisphosphate receptor inhibits the progression of pulmonary arterial hypertension via calcium signaling and apoptosis. Heart Vessels. 2019;34:724–34.
13. Rosa N, Ivanova H, Wagner LE 2nd, Kale J, La Rovere R, Welkenhuyzen K, Louros N, Karamanou S, Shabardina V, Lemmens I, et al. Bcl-xL acts as an inhibitor of IP(3)R channels, thereby antagonizing Ca(2+)-driven apoptosis. Cell Death Differ. 2022;29:788–805.
14. Woll KA, Van Petegem F. Calcium-release channels: structure and function of IP(3) receptors and Ryanodine receptors. Physiol Rev. 2022;102:209–68.
15. Avalle L, Camporeale A, Morciano G, Caroccia N, Ghetti E, Orecchia V, Viavattene D, Giorgi C, Pinton P, Poli V. STAT3 localizes to the ER, acting as a gatekeeper for ER-mitochondrion Ca(2+) fluxes and apoptotic responses. Cell Death Differ. 2019;26:932–42.
16. Xu Y, Guo X, Ning S, He Q, Meng B, Xing F, Yin Y. Inhibition of IP(3)R3 attenuates endothelial to mesenchymal transition induced by TGF-β1 through restoring mitochondrial function. Biochem Biophys Res Commun. 2022;619:144–50.
17. Wang S, Ge W, Harns C, Meng X, Zhang Y, Ren J. Ablation of toll-like receptor 4 attenuates aging-induced myocardial remodeling and contractile dysfunction through NCoRI-HDAC1-mediated regulation of autophagy. J Mol Cell Cardiol. 2018;119:40–50.
18. Liu Y, Ma X, Fujioka H, Liu J, Chen S, Zhu X. DJ-1 regulates the integrity and function of ER-mitochondria association through interaction with IP3R3-Grp75-VDAC1. Proc Natl Acad Sci U S A. 2019;116:25322–28.
19. Cheng X, Wang Y, Chen H, Xu Y, Xiong W, Wang T. Claudin-1 regulates pulmonary artery smooth muscle cell proliferation through the activation of ERK1/2. Biomed Pharmacother. 2017;89:983–90.
20. Groenendyk J, Agellon LB, Michalak M. Calcium signaling and Endoplasmic reticulum stress. Int Rev Cell Mol Biol. 2021;363:1–20.
21. Hajnóczky G, Csordás G, Madesh M, Pacher P. The machinery of local Ca2 + signalling between sarco-endoplasmic reticulum and mitochondria. J Physiol. 2000;529(Pt):69–81.
22. Masson B, Le Ribeuz H, Sabourin J, Laubry L, Woodhouse E, Foster R, Ruchon Y, Dutheil M, Boët A, Ghigna MR, et al. Orai1 inhibitors as potential treatments for pulmonary arterial hypertension. Circ Res. 2022;131:e102–19.
23. Li L, Liu B, Zhang H, Wang C, Sun L, Zhang Y, Song L, Yu Y, Zhou K. 4-Phenylbutyric acid suppresses psoralen-induced hepatotoxicity by inhibiting ERS and reestablishing mitochondrial fusion-fission balance in mice. Toxicology. 2024;509:153954.
24. Wu Y, Yan QZ, Wang J, Zhang MF, Wang R, Wang SC. Effect of Endoplasmic reticulum stress-mitochondrial autophagy pathway on pulmonary hypertension in rats. Chin J Comp Med. 2022;32:53–9.
25. Karalliedde LD, Kappagoda CT. The challenge of traditional Chinese medicines for allopathic practitioners. Am J Physiol Heart Circ Physiol. 2009;297:H1967–1969.
26. Yu Q, Li X, Cao X. Cardioprotective effects of phenylethanoid Glycoside-rich extract from Cistanche deserticola in Ischemia-Reperfusion-Induced myocardial infarction in rats. Ann Vasc Surg. 2016;34:234–42.
27. Hassoun PM. Pulmonary arterial hypertension. N Engl J Med. 2021;385:2361–76.
28. Chen J, Luo J, Qiu H, Tang Y, Yang X, Chen Y, Li Z, Li J. Apolipoprotein A5 ameliorates MCT induced pulmonary hypertension by inhibiting ER stress in a GRP78 dependent mechanism. Lipids Health Dis. 2022;21:69.
29. Hu XQ, Zhang L. Hypoxia and the integrated stress response promote pulmonary hypertension and preeclampsia: implications in drug development. Drug Discov Today. 2021;26:2754–73.
30. Zhang Q, Chen Y, Wang Q, Wang Y, Feng W, Chai L, Liu J, Li D, Chen H, Qiu Y, et al. HMGB1-induced activation of ER stress contributes to pulmonary artery hypertension in vitro and in vivo. Respir Res. 2023;24:149.
31. Wu Y, Adi D, Long M, Wang J, Liu F, Gai MT, Aierken A, Li MY, Li Q, Wu LQ, et al. 4-Phenylbutyric acid induces protection against pulmonary arterial hypertension in rats. PLoS ONE. 2016;11:e0157538.
32. Chen Y, Csordás G, Jowdy C, Schneider TG, Csordás N, Wang W, Liu Y, Kohlhaas M, Meiser M, Bergem S, et al. Mitofusin 2-containing mitochondrial-reticular microdomains direct rapid cardiomyocyte bioenergetic responses via interorganelle Ca(2+) crosstalk. Circ Res. 2012;111:863–75.
33. Bartok A, Weaver D, Golenár T, Nichtova Z, Katona M, Bánsághi S, Alzayady KJ, Thomas VK, Ando H, Mikoshiba K, et al. IP(3) receptor isoforms differently regulate ER-mitochondrial contacts and local calcium transfer. Nat Commun. 2019;10:3726.
34. Hong Z, Chen KH, DasGupta A, Potus F, Dunham-Snary K, Bonnet S, Tian L, Fu J, Breuils-Bonnet S, Provencher S, et al. MicroRNA-138 and MicroRNA-25 Down-regulate mitochondrial calcium uniporter, causing the pulmonary arterial hypertension cancer phenotype. Am J Respir Crit Care Med. 2017;195:515–29.
35. Mendes CC, Gomes DA, Thompson M, Souto NC, Goes TS, Goes AM, Rodrigues MA, Gomez MV, Nathanson MH, Leite MF. The type III inositol 1,4,5-trisphosphate receptor preferentially transmits apoptotic Ca2 + signals into mitochondria. J Biol Chem. 2005;280:40892–900.
36. Rizzuto R, De Stefani D, Raffaello A, Mammucari C. Mitochondria as sensors and regulators of calcium signalling. Nat Rev Mol Cell Biol. 2012;13:566–78.
37. Di Rienzo M, Romagnoli A, Ciccosanti F, Refolo G, Consalvi V, Arena G, Valente EM, Piacentini M, Fimia GM. AMBRA1 regulates mitophagy by interacting with ATAD3A and promoting PINK1 stability. Autophagy. 2022;18:1752–62.
38. Xu H, Zhang J, Zhou Y, Zhao G, Cai M, Gao J, Shao L, Shi Y, Li H, Ji H et al. Mechanistic Insights into Membrane Protein Clustering Revealed by Visualizing EGFR Secretion. *Research (Wash D C)* 2022, 2022:9835035.
39. Larsen BD, Madsen MR, Nielsen R, Mandrup S. Chromatin Immunoprecipitation for identification of Protein-DNA interactions in human cells. Methods Mol Biol. 2018;1794:335–52.
40. Patten DK, Corleone G, Magnani L. Chromatin Immunoprecipitation and High-Throughput sequencing (ChIP-Seq): tips and tricks regarding the laboratory protocol and initial downstream data analysis. Methods Mol Biol. 2018;1767:271–88.
41. Chen SZ, Ling Y, Yu LX, Song YT, Chen XF, Cao QQ, Yu H, Chen C, Tang JJ, Fan ZC, et al. 4-phenylbutyric acid promotes hepatocellular carcinoma via

initiating cancer stem cells through activation of PPAR-α. Clin Transl Med. 2021;11:e379.
42. Guo Q, Xu L, Li H, Sun H, Wu S, Zhou B. 4-PBA reverses autophagic dysfunction and improves insulin sensitivity in adipose tissue of obese mice via Akt/mTOR signaling. Biochem Biophys Res Commun. 2017;484:529–35.
43. Koyama M, Furuhashi M, Ishimura S, Mita T, Fuseya T, Okazaki Y, Yoshida H, Tsuchihashi K, Miura T. Reduction of Endoplasmic reticulum stress by 4-phenylbutyric acid prevents the development of hypoxia-induced pulmonary arterial hypertension. Am J Physiol Heart Circ Physiol. 2014;306:H1314–1323.
44. Kolb PS, Ayaub EA, Zhou W, Yum V, Dickhout JG, Ask K. The therapeutic effects of 4-phenylbutyric acid in maintaining proteostasis. Int J Biochem Cell Biol. 2015;61:45–52.
45. Periasamy M, Huke S. SERCA pump level is a critical determinant of Ca(2+) homeostasis and cardiac contractility. J Mol Cell Cardiol. 2001;33:1053–63.
46. Liu Y, Zhang H, Liu Y, Zhang S, Su P, Wang L, Li Y, Liang Y, Wang X, Zhao W, et al. Hypoxia-induced GPCPD1 depalmitoylation triggers mitophagy via regulating PRKN-mediated ubiquitination of VDAC1. Autophagy. 2023;19:2443–63.
47. Bers DM. Cardiac excitation-contraction coupling. Nature. 2002;415:198–205.
48. Zhong M, Karma A. Role of Ryanodine receptor cooperativity in Ca(2+)-wave-mediated triggered activity in cardiomyocytes. J Physiol. 2024;602:6745-87.
49. Marks AR. Targeting Ryanodine receptors to treat human diseases. J Clin Invest. 2023;133:e162891.
50. Hadiatullah H, He Z, Yuchi Z. Structural insight into Ryanodine receptor channelopathies. Front Pharmacol. 2022;13:897494.
51. Dridi H, Kushnir A, Zalk R, Yuan Q, Melville Z, Marks AR. Intracellular calcium leak in heart failure and atrial fibrillation: a unifying mechanism and therapeutic target. Nat Rev Cardiol. 2020;17:732–47.
52. Gleitze S, Ramírez OA, Vega-Vásquez I, Yan J, Lobos P, Bading H, Núñez MT, Paula-Lima A, Hidalgo C. Ryanodine receptor mediated calcium release contributes to ferroptosis induced in primary hippocampal neurons by GPX4 Inhibition. Antioxid (Basel). 2023;12:705.
53. Zhao YT, Valdivia CR, Gurrola GB, Hernández JJ, Valdivia HH. Arrhythmogenic mechanisms in Ryanodine receptor channelopathies. Sci China Life Sci. 2015;58:54–8.
54. Dulhunty AF. Molecular changes in the cardiac RyR2 with catecholaminergic polymorphic ventricular tachycardia (CPVT). Front Physiol. 2022;13:830367.
55. Zheng YM, Wang QS, Rathore R, Zhang WH, Mazurkiewicz JE, Sorrentino V, Singer HA, Kotlikoff MI, Wang YX. Type-3 Ryanodine receptors mediate hypoxia-, but not neurotransmitter-induced calcium release and contraction in pulmonary artery smooth muscle cells. J Gen Physiol. 2005;125:427–40.
56. Mei L, Zheng YM, Song T, Yadav VR, Joseph LC, Truong L, Kandhi S, Barroso MM, Takeshima H, Judson MA, Wang YX. Rieske iron-sulfur protein induces FKBP12.6/RyR2 complex remodeling and subsequent pulmonary hypertension through NF-κB/cyclin D1 pathway. Nat Commun. 2020;11:3527.
57. Westcott EB, Goodwin EL, Segal SS, Jackson WF. Function and expression of Ryanodine receptors and inositol 1,4,5-trisphosphate receptors in smooth muscle cells of murine feed arteries and arterioles. J Physiol. 2012;590:1849–69.
58. McGeown JG. Interactions between inositol 1,4,5-trisphosphate receptors and Ryanodine receptors in smooth muscle: one store or two? Cell Calcium. 2004;35:613–19.

Publisher's note